

CHAPTER 5	57
RESULTS FOR SEXTET TRANSITIONS.....	57
IN O IV, F V AND NE VI	57
5.1 THE $1s2s2p^23s\ ^6P-1s2p^33s\ ^6S^o$ TRANSITIONS IN O IV, F V AND NE VI.....	57
5.1.1 The $1s2s2p^23s\ ^6P-1s2p^33s\ ^6S^o$ Transitions in O IV.	58
5.1.2 The $1s2s2p^23s\ ^6P-1s2p^33s\ ^6S^o$ Transitions in F V.	60
5.1.3 The $1s2s2p^23s\ ^6P-1s2p^33s\ ^6S^o$ Transitions in Ne VI.	62
5.1.4. COMPARISON OF THE $1s2s2p^23s\ ^6P-1s2p^33s\ ^6S^o$ TRANSITIONS WITH THEORY ALONG ISOELECTRONIC SEQUENCE.....	63
5.1.5. Summary.....	69
5.2 THE $1s2s2p^23p\ ^6L^o-1s2p^33p\ ^6P$, L=S, P, D TRANSITIONS IN O IV, F V AND NE VI.....	71
5.2.1 The $1s2s2p^23p\ ^6L^o-1s2p^33p\ ^6P$ transitions in O IV.	73
5.2.3 The $1s2s2p^23p\ ^6L^o-1s2p^33p\ ^6P$ transitions in Ne VI.	76
5.2.4 Comparison of the $1s2s2p^23p\ ^6L^o-1s2p^33p\ ^6P$ Transitions with Theory Along Isoelectronic Sequence.....	77
5.2.5. Summary.....	85
5.3 THE $1s2s2p^23d\ ^6L-1s2p^33d\ ^6D^o$, L=P, D, F TRANSITIONS IN O IV, F V AND NE VI.....	86
5.3.1 The $1s2s2p^23d\ ^6L-1s2p^33d\ ^6D^o$ transitions in O IV.	86
5.3.2 The $1s2s2p^23d\ ^6L-1s2p^33d\ ^6D^o$ transitions in F V.	92
5.3.3 The $1s2s2p^23d\ ^6L-1s2p^33d\ ^6D^o$ transitions in Ne VI.	94
5.3.4 Comparisons with Theory of the $1s2s2p^23d\ ^6L-1s2p^33d\ ^6D$ Transitions along B I Isoelectronic Sequence.....	96
5.3.5. Summary.....	104

FIG.5.1.1. THE TRANSITIONS IN THE BEAM-FOIL SPECTRA OF OXYGEN, FLUORINE AND NEON, RECORDED AT THE DIFFERENT ENERGIES. THE BEAM ENERGIES AND SPECTROMETER SLIT WIDTHS ARE SHOWN.	59
FIG. 5.1.2. SCALED ISOELECTRONIC PLOT OF THE CENTER OF GRAVITY WAVELENGTH (A) AND TRANSITION ENERGY DEVIATIONS FROM EXPERIMENT (B) OF THE $1s2s2p^23s\ ^6P-1s2p^33s\ ^6S^o$ MULTIPLET TRANSITIONS FOR THE BORON SEQUENCE. THE EXPERIMENTAL AND CALCULATED POINTS ARE DENOTED BY THE FOLLOWING: CIRCLES WITH ERROR BARS INSIDE FOR EXPERIMENTS, + FOR SCHF, o FOR SCHFT, FOR MCHF, * FOR MCHFT, Δ FOR SCDF, AND DIAMONDS FOR MCDF.....	65
FIG. 5.1.3. COMPARISON OF THE EXPERIMENTAL (OPENED CIRCLES) AND THEORETICAL (OTHERS) FINE STRUCTURES FOR O IV, FV AND Ne VI. THE EXPERIMENTAL AND CALCULATED POINTS ARE DENOTED BY THE FOLLOWING: CIRCLES WITH ERROR BARS INSIDE FOR EXPERIMENTS, Δ FOR SCHFT, □ FOR MCHFT, DIAMONDS FOR SCDF, AND * FOR MCDF	66
FIG. 5.1.4. ISOELECTRONIC COMPARISON OF THE QED EFFECTS AND HIGHER-ORDER CORRECTIONS OF THE $1s2s2p^23s\ ^6P-1s2p^33s\ ^6S^o$ TRANSITIONS FOR THE BORON SEQUENCE. THE CALCULATED POINTS ARE DENOTED BY THE FOLLOWING: DIAMONDS FOR QED EFFECTS FROM SCHF, Δ FOR HIGHER ORDER CORRECTIONS FROM SCHF, o FOR QED EFFECTS FROM MCHF, AND □ FOR HIGHER ORDER CORRECTIONS FROM MCHF. THE FITTED QED EFFECTS FROM BOTH SCHF AND MCHF ARE DENOTED BY SOLID LINE.....	67
FIG. 5.1.5. ISOELECTRONIC COMPARISON OF THE THEORETICAL AND EXPERIMENTAL MEAN WAVELENGTHS OF THE $1s2s2p^23s\ ^6P-1s2p^33s\ ^6S^o$ TRANSITIONS FOR THE BORON SEQUENCE.	68
FIG. 5.2.1. THE $1s2s2p^23p\ ^6L$ AND $1s2p^33p\ ^6P$ TRANSITIONS IN THE BEAM-FOIL SPECTRA OF OXYGEN, FLUORINE AND NEON, RECORDED AT THE DIFFERENT ENERGIES. THE BEAM ENERGIES AND SPECTROMETER SLIT WIDTHS ARE INDICATED.	72
FIG. 5.2.2. THE IDENTIFICATIONS OF THE $1s2s2p^23p\ ^6D_j-1s2p^33p\ ^6P_j$ AND $1s2s2p^23p\ ^6S_{5/2}-1s2p^33p\ ^6P_j$ TRANSITIONS OF O IV IN THE EXPERIMENTAL SPECTRUM OF O AT THE ENERGY OF 2.5 MeV. IN (A) * MEANS ALL POSSIBLE J'S OF THE UPPER STATES ALLOWED BY E1 TRANSITION RULES. IN (B) * MEANS 3/2, 5/2 AND 7/2.	75
82	

FIG. 5.2.3. THE DEVIATIONS BETWEEN THE THEORETICAL AND EXPERIMENTAL TRANSITION ENERGIES FOR THE $1s2s2p^23p\ ^6D_J-1s2p^33p\ ^6P_J$ TRANSITIONS. HERE THE THEORETICAL TRANSITION ENERGY IS THE CENTER OF GRAVITY OF THE $1s2s2p^23p\ ^6D_J-1s2p^33p\ ^6P_J$ TRANSITION ENERGIES (COMPUTED FROM THE FINE STRUCTURE LINES BY THIS WORK) WITH THE RESULTS OF THEORETICAL ANALYSIS, AND THE EXPERIMENTAL TRANSITION ENERGY IS THE CENTER OF GRAVITY OF THE $1s2s2p^23p\ ^6D_J-1s2p^33p\ ^6P_J$ TRANSITION ENERGIES (COMPUTED FROM THE OBSERVED LINES) WITH THE RESULTS OF THEORETICAL ANALYSIS.....	82
FIG. 5.2.4. THE DEVIATIONS BETWEEN THE THEORETICAL AND EXPERIMENTAL TRANSITION ENERGIES FOR THE $1s2s2p^23p\ ^6P_J-1s2p^33p\ ^6P_J$ TRANSITIONS. HERE THE THEORETICAL TRANSITION ENERGY IS THE CENTER OF GRAVITY OF THE $1s2s2p^23p\ ^6P_J-1s2p^33p\ ^6P_J$ TRANSITION ENERGIES (COMPUTED FROM THE FINE STRUCTURE LINES BY THIS WORK) WITH THE RESULTS OF THEORETICAL ANALYSIS, AND THE EXPERIMENTAL TRANSITION ENERGY IS THE CENTER OF GRAVITY OF THE $1s2s2p^23p\ ^6P_J-1s2p^33p\ ^6P_J$..	82
TRANSITION ENERGIES (COMPUTED FROM THE OBSERVED LINES) WITH THE RESULTS OF THEORETICAL ANALYSIS.....	82
FIG. 5.2.5. THE DEVIATIONS BETWEEN THE THEORETICAL AND EXPERIMENTAL TRANSITION ENERGIES FOR THE $1s2s2p^23p\ ^6S_J-1s2p^33p\ ^6P_J$ TRANSITIONS. HERE THE THEORETICAL TRANSITION ENERGY IS THE CENTER OF GRAVITY OF THE $1s2s2p^23p\ ^6S_J-1s2p^33p\ ^6P_J$ TRANSITION ENERGIES (COMPUTED FROM THE FINE STRUCTURE LINES BY THIS WORK) WITH THE RESULTS OF THEORETICAL ANALYSIS, AND THE EXPERIMENTAL TRANSITION ENERGY IS THE CENTER OF GRAVITY OF THE $1s2s2p^23p\ ^6S_J-1s2p^33p\ ^6P_J$ TRANSITION ENERGIES (COMPUTED FROM THE OBSERVED LINES) WITH THE RESULTS OF THEORETICAL ANALYSIS.....	83
FIG. 5.2.6. THE QED AND HIGHER-ORDER CORRECTIONS FOR (A) THE $1s2s2p^23p\ ^6D-1s2p^33p\ ^6P$, (B) $1s2s2p^23p\ ^6P-1s2p^33p\ ^6P$ AND (C) $1s2s2p^23p\ ^6S-1s2p^33p\ ^6P$ TRANSITIONS IN THE B I ISOELECTRONIC SEQUENCE.	84
FIG. 5.3.2. THE $1s2s2p^23d\ ^6L_J - 1s2p^33d\ ^6D_J$, L=P, D, F TRANSITIONS IN THE BEAM-FOIL SPECTRA OF OXYGEN, FLUORINE AND NEON, RECORDED AT DIFFERENT ENERGIES. THE BEAM ENERGIES AND SPECTROMETER SLIT WIDTHS IN ARE INDICATED.	88
FIG. 5.3.2. THE IDENTIFICATIONS OF THE $1s2s2p^23d\ ^6F_J - 1s2p^33d\ ^6D_J$ TRANSITIONS OF O IV IN THE EXPERIMENTAL SPECTRUM OF $^{20}O^+$ AT THE ENERGY OF 2.5 MEV.	91
97	
FIG. 5.3.3. THE DEVIATIONS BETWEEN THE THEORETICAL AND EXPERIMENTAL TRANSITION ENERGIES FOR THE $1s2s2p^23d\ ^6F-1s2p^33d\ ^6D$ TRANSITIONS.	97
FIG. 5.3.4. THE DEVIATIONS BETWEEN THE THEORETICAL AND EXPERIMENTAL TRANSITION ENERGIES FOR THE $1s2s2p^23d\ ^6D-1s2p^33d\ ^6D$ TRANSITIONS.	98
98	
FIG. 5.3.5. THE DEVIATIONS BETWEEN THE THEORETICAL AND EXPERIMENTAL TRANSITION ENERGIES FOR THE $1s2s2p^23d\ ^6P-1s2p^33d\ ^6D$ TRANSITIONS.	98
99	
FIG. 5.3.6. THE REDUCED EXPERIMENTAL TRANSITION ENERGIES $\delta E/(Z-1.86)$ FOR THE $1s2s2p^23d\ ^6F_J-1s2p^33d\ ^6D_J$ TRANSITIONS.	99
FIG. 5.3.7. THE REDUCED EXPERIMENTAL TRANSITION ENERGIES $\delta E/(Z-1.86)$ FOR THE $1s2s2p^23d\ ^6D_J-1s2p^33d\ ^6D_J$ TRANSITIONS.	99
100	
FIG. 5.3.8. THE REDUCED EXPERIMENTAL TRANSITION ENERGIES $\delta E/(Z-1.86)$ FOR THE $1s2s2p^23d\ ^6P_J-1s2p^33d\ ^6D_J$ TRANSITIONS.	100
FIG. 5.3.9 THE LIFETIMES (IN PS) FOR THE $1s2s2p^23d\ ^6P^E$ STATES IN THE BORON SEQUENCE. EXPERIMENTAL VALUES ARE TAKEN FROM TABLE 5.3.5.	101
FIG. 5.3.10 THE LIFETIMES (IN PS) FOR THE $1s2p^33d\ ^6D^O$ STATES IN THE BORON SEQUENCE.....	102
FIG. 5.3.11. THE QED AND HIGHER-ORDER CORRECTIONS FOR (A) THE $1s2s2p^23d\ ^6F-1s2p^33d\ ^6D$, (B) $1s2s2p^23d\ ^6D-1s2p^33d\ ^6D$ AND (C) $1s2s2p^23d\ ^6P-1s2p^33d\ ^6D$ TRANSITIONS IN THE B I ISOELECTRONIC SEQUENCE.	103

TABLE 5.1.1. THE ENERGIES (IN CM-1) AND WAVELENGTHS (IN Å) FOR $1s2s2p^23s\ ^6P_J-1s2p^33s\ ^6S^o_{5/2}$ TRANSITIONS IN O IV, F V, AND NE VI BY THIS WORK. HERE WE ALSO LIST THE QED EFFECTS AND

HIGHER-ORDER CORRECTIONS FOR THE $1s2s2p^23s\ ^6P_J-1s2p^33s\ ^6S^o_{5/2}$ TRANSITIONS IN O IV, F V, AND NE VI. THE ERRORS FOR CALCULATIONS ARE ROOT MEAN SQUARE DIFFERENCES BETWEEN THE CALCULATED AND EXPERIMENTAL VALUES.	61
TABLE 5.1.2. FINE STRUCTURE (IN CM^{-1}) OF THE $1s2s2p^23s\ ^6P_J$ STATES IN O IV, F V AND NE VI.	64
TABLE 5.1.3. LIFETIME (IN PS) OF THE $1s2s2p^23s\ ^6P$ AND $1s2p^33s\ ^6S^o_{5/2}$ STATES IN O IV, F V AND NE VI. ..	64
TABLE 5.1.4. ELECTRON SCREENING Σ FOR THE 2S AND 2P VALENCE ELECTRON OF THE $1s2s2p^23s\ ^6P$ AND $1s2p^33s\ ^6S^o_{5/2}$ STATES IN O IV, F V AND NE VI.	64
TABLE 5.2.1. THE ENERGIES E (IN CM^{-1}) AND WAVELENGTHS λ (IN \AA) FOR THE $1s2s2p^23p\ ^6L_J-1s2p^33p\ ^6P_J$ TRANSITIONS IN O IV, F V AND NE VI BY THIS WORK. WE ALSO LIST THE DEVIATIONS BETWEEN THE THEORETICAL AND EXPERIMENTAL TRANSITION ENERGIES FOR THE $1s2s2p^23p\ ^6L_J-1s2p^33p\ ^6P_J$ TRANSITIONS.	78
TABLE 5.2.1. (CONTINUED)	79
TABLE 5.2.1. (CONTINUED)	80
TABLE 5.3.1. THE ENERGIES E (IN CM^{-1}) AND WAVELENGTHS λ (IN \AA) FOR THE $1s2s2p^23d\ ^6L_J-1s2p^33d\ ^6D_J$ TRANSITIONS IN O IV BY THIS WORK. WE ALSO LIST THE DEVIATIONS BETWEEN THE THEORETICAL AND EXPERIMENTAL TRANSITION ENERGIES FOR THE $1s2s2p^23d\ ^6L_J-1s2p^33d\ ^6D_J$ TRANSITIONS.	89
TABLE 5.3.2. THE WAVELENGTHS λ (IN \AA) FOR THE $1s^22p3p\ ^1D_2-1s^22p4d\ ^1F_3$ TRANSITIONS IN O V BY THIS WORK.	91
TABLE 5.3.3. THE ENERGIES E (IN CM^{-1}) AND WAVELENGTHS λ (IN \AA) FOR THE $1s2s2p^23d\ ^6L_J-1s2p^33d\ ^6D_J$ TRANSITIONS IN F V BY THIS WORK. WE ALSO LIST THE DEVIATIONS BETWEEN THE THEORETICAL AND EXPERIMENTAL TRANSITION ENERGIES FOR THE $1s2s2p^23d\ ^6L_J-1s2p^33d\ ^6D_J$ TRANSITIONS.	93
TABLE 5.3.4. THE ENERGIES E (IN CM^{-1}) AND WAVELENGTHS λ (IN \AA) FOR THE $1s2s2p^23d\ ^6L_J-1s2p^33d\ ^6D_J$ TRANSITIONS IN NE VI BY THIS WORK. WE ALSO LIST THE DEVIATIONS BETWEEN THE THEORETICAL AND EXPERIMENTAL TRANSITION ENERGIES FOR THE $1s2s2p^23d\ ^6L_J-1s2p^33d\ ^6D_J$ TRANSITIONS.....	95
TABLE 5.3.5. LIFETIMES (IN PS) OF THE $1s2s2p^23d\ ^6P$ AND $1s2p^33d\ ^6D$ STATES IN N III, O IV, F V, NE VI AND NA VII.....	101

CHAPTER 5
RESULTS FOR SEXTET TRANSITIONS
IN O IV, F V AND NE VI

The main aim of this work is to give a perspective of the current understanding of the doubly excited sextet states $1s2s2p^23l\ ^6L$ and $1s2p^33l\ ^6L'$, $l=s, p, d$ in O IV.

Using the above theory and experimental considerations, we have studied the fast beam-foil spectra of oxygen were recorded at a van de Graaff accelerator at Liège using a Seya-Nomioka grating incidence spectrometer. The $1s2s2p^23l\ ^6L$ - $1s2p^33l\ ^6L'$, $l=s, p, d$, electric-dipole transitions between sextet states in O IV, F V and Ne VI have been searched in these spectra and in spectra previously recorded at Lyon and Argonne. At the same time we also find some new electric-dipole transitions in doubly excited O V and reassign some electric-dipole transitions in doubly excited O V. The results will be presented below.

5.1 The $1s2s2p^23s\ ^6P$ - $1s2p^33s\ ^6S^o$ Transitions In O IV, F V And Ne VI.

The transitions from doubly excited states appear as weak lines among a rich collection of other unidentified lines of highly excited oxygen, fluorine and neon [115-120]. Fig. 5.1.1 shows 5 spectra recorded in the wavelength regions of interest. Initial peak locations were found using non-linear least squared fits to Gaussian profiles. The wavelength measurement procedures and results for each set of transitions are described in more detail below.

5.1.1 The $1s2s2p^23s\ ^6P-1s2p^33s\ ^6S^o$ Transitions in O IV.

We obtained spectra at several different ion beam energies in the wavelength region where the sextet transitions $1s2s2p^23s\ ^6P-1s2p^33s\ ^6S^o$ in O IV were expected. Three typical spectra are shown in Fig. 5.1.1(a), 5.1.1(b) and 5.1.1(c). A promising candidate for the transition at $656.58\pm0.08\ \text{\AA}$ remains at 1.7 and 2.5 MeV O^+ ion beam energy and has much weaker intensity at 1.2 MeV O_2^+ ion beam energy. The strong 3d-4f and 3p-4d transitions of beryllium-like O V are seen at $654.72\ \text{\AA}$ and $659.60\ \text{\AA}$. The two wavelengths have been semiempirically determined with an accuracy $\pm0.004\ \text{\AA}$ by [121-123] and provide a good calibration for our measurements. The standard error for wavelength calibration is $0.01\ \text{\AA}$ in the region of 650-670 \AA . Nonlinear least square fits of Gaussian profiles give the values for the wavelengths, intensities and full widths at half maximum (FWHM) of lines. The uncertainties of the wavelengths are related to the intensities of the lines. The precision of the profile-fitting program was also checked through the all known transition wavelengths. The fitted curves are shown in the Figs. 5.1.1(b) and 5.1.1(c).

For the $1s2s2p^23s\ ^6P_J-1s2p^33s\ ^6S^o$ transitions we expected to resolve the fine structures in our experiments. The strongest transition related to fine structure components is the $J=7/2-5/2$ transition at the wavelength of $656.58\pm0.08\ \text{\AA}$. We also obtained the wavelength for the $J=5/2-5/2$ transition at $655.50\pm0.10\ \text{\AA}$. The $J=3/2-5/2$ transition at $654.02\ \text{\AA}$ is weak and blended with the strong 3d-4f transitions of O V at the ion energy of 1.7MeV in Fig. 5.1.1(b), where it is hard to deconvolute the line from the strong 3d-4f transitions and the relative intensities are difficult to compare. We estimated that the wavelength of the $J=3/2-5/2$ transition is $654.02\pm0.10\ \text{\AA}$ by fitting the spectrum at the energy of 2.5 MeV in

Fig. 5.1.1(c). The transition rate is proportional to the area of the peak (the fitted intensity \times FWHM of the experiments). The ratio of the $J=7/2-5/2$ and $J=5/2-5/2$ transition rates at the ion energy of 1.7 MeV in Fig. 5.1.1(b) is found to be about $167\times 0.7:124\times 0.7 = 4.06:3$, and is consistent with the theoretical value 8:6 if we ignore other small differences. The ratios of the $J=7/2-5/2$, $J=5/2-5/2$ and $J=3/2-5/2$ transition rates at the energy of 2.5 MeV in Fig. 5.1.1(c) are about 7.7:5.9:4.0. Within experimental error, these ratios are consistent with the theoretical values of 8:6:4. In Table 5.1.1 we present our measured fine structure wavelength values and compare them with our different theoretical values for O IV. The associated fine structures of the lower state $1s2s2p^23s\ ^6P_J$ for $J=7/2-5/2$ and $J=5/2-3/2$ are $254\pm 19\text{ cm}^{-1}$ and $345\pm 19\text{ cm}^{-1}$ listed in Table 5.1.2, and are consistent with our calculations.

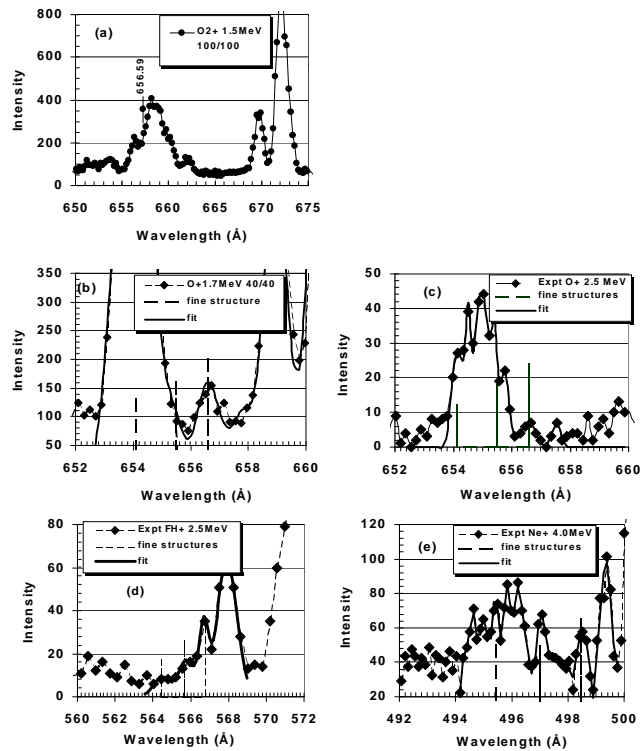


FIG. 5.1.1. The transitions in the beam-foil spectra of oxygen, fluorine and neon recorded at the different energies. The beam energies and spectrometer slit widths are shown.

5.1.2 The $1s2s2p^23s\ ^6P-1s2p^33s\ ^6S^o$ Transitions in F V.

Fig. 5.1.1(d) shows the spectrum of $^{20}(\text{FH})^+$ for a beam energy of 2.5 MeV recorded at Lyon, France. Many unidentified lines are located in the wavelength region where the sextet lines were expected. In addition, the $1s^24f-1s^26g$ transition of lithium-like F VII at 535.52 Å and the $2s^22p^2-2s2p^3$ transitions of carbon-like F IV at 572.66 Å are observed. These wavelengths have previously been determined with an accuracy ± 0.026 Å and ± 0.003 Å by Moore and Engström et al [124,125] and help to provide a good calibration for our measurements. The same experimental procedures and programs described as 4.1 were applied to analyze the spectrum for F V. The standard error for wavelength calibration is 0.03 Å in the region of 562-575 Å. The spectroscopic linewidths were about 0.8 Å. The fitted curve is shown in the Fig. 5.1.1(d).

For the $1s2s2p^23s\ ^6P_J-1s2p^33s\ ^6S^o$ transitions we also expected to resolve the fine structures in our experiments. However, as shown in Fig. 5.1.1(d), the count rates of the expected lines in the wavelength region near 562-575 Å are very low. The wavelengths for the $J=7/2, 5/2, 3/2-5/2$ transitions are 566.70 ± 0.15 Å, 565.51 ± 0.15 Å and 564.34 ± 0.15 Å, respectively with the slightly large error bars. The ratios of the three transition rates are found to be about 7.8:5.9:4.0. They are consistent with the theoretical values of 8:6:4 within experimental precision. In Table 5.1.1 we present our measured fine structure wavelength values and compare these with our theoretical values for F V. The associated fine structures of the lower state $1s2s2p^23s\ ^6P_J$ for $J=7/2-5/2$ and $J=5/2-3/2$ are $371\pm 38\text{ cm}^{-1}$ and $367\pm 38\text{ cm}^{-1}$ listed in Table 5.1.2. They are consistent with our calculations.

TABLE 5.1.1. The energies (in cm^{-1}) and wavelengths (in \AA) for $1s2s2p^23s\ ^6P_J-1s2p^33s\ ^6S^o_{5/2}$ transitions in O IV, F V, and Ne VI by this work. Here we also list the QED effects and higher-order corrections for the $1s2s2p^23s\ ^6P_J-1s2p^33s\ ^6S^o_{5/2}$ transitions in O IV, F V, and Ne VI. The errors for calculations are root mean square differences between the calculated and experimental values.

Z	J	Experiment	E_{SCHF}	E_{SCHF}^T	E_{MCHF}	E_{MCHF}^T	E_{SCDF}	E_{MCDF}	units	
8	Av	(152519±23)	152175.4	152280.7	151885.8	152034.3	149538.7	152091.9	cm^{-1}	
		655.66±0.10	657.14	656.68	658.39	657.75	668.72	657.50	\AA	
	7/2	152302±19	152036.2	152153.3	151746.9	151788.7	149547.1	151879.1	cm^{-1}	
			656.58±0.08	657.74	657.23	658.99	658.81	668.69	658.42	\AA
		5/2	152505±23	152196.8	152410.6	151907.4	152034.1	149372.6	152147.0	cm^{-1}
				655.50±0.10	657.04	656.12	658.30	657.75	669.47	657.26
	3/2	(152901±23)	152421.7	152753.5	152131.4	152280.4	149770.8	152434.9	cm^{-1}	
			(654.02±0.10)	656.07	654.65	657.33	656.68	667.69	656.02	\AA
	9	Av	176747±47	176543.0	176595.5	176399.8	176336.7	173947.1	176152.2	cm^{-1}
			565.78±0.15	566.43	566.27	566.89	567.10	574.89	567.69	\AA
		7/2	176460±47	176327.9	176374.7	176132.7	176091.0	173913.5	175941.3	cm^{-1}
				566.70±0.15	567.13	566.97	567.75	567.89	575.00	568.37
5/2			176832±47	176651.4	176860.5	176455.3	176223.2	173916.4	176190.7	cm^{-1}
				565.51±0.15	566.09	565.42	566.72	567.46	574.99	567.57
3/2		177198±47	177049.1	177268.4	176851.3	176736.0	174060.3	176516.4	cm^{-1}	
			564.34±0.15	564.82	564.12	565.45	565.82	574.51	566.52	\AA
10		Av	201054±20	201081.3	200878.0	200922.6	201117.9	199161.2	201401.3	cm^{-1}
			497.38±0.05	497.31	497.81	497.70	497.22	502.11	496.52	\AA
		7/2	200586±20	200613.0	200522.8	200455.9	200627.2	198572.6	200793.0	cm^{-1}
				498.54±0.05	498.47	498.70	498.86	498.44	503.59	498.03
	5/2		201175±20	201194.1	201127.4	201035.1	201371.0	199326.0	201575.3	cm^{-1}
				497.08±0.05	497.03	497.20	497.43	496.60	501.69	496.09
	3/2	201820±20	201848.8	201887.7	201688.1	201838.2	200091.1	202357.0	cm^{-1}	
			495.49±0.05	495.42	495.32	495.82	495.45	499.77	494.18	\AA
									cm^{-1}	
									cm^{-1}	

5.1.3 The $1s2s2p^23s\ ^6P-1s2p^33s\ ^6S^o$ Transitions in Ne VI.

The same experimental procedures and programs were applied to analyze the spectrum for Ne VI. The spectrum was recorded at the Argonne National Lab Dynamitron Accelerator [Berry and Livingston, data 1988, unpublished]. Fig. 5.1.1(e) shows the 2nd order spectrum of neon from a beam of $^{20}\text{Ne}^+$ at an energy of 4 MeV. In the wavelength region where the sextet lines were expected many unidentified lines are located as well as the nearby $1s4d-1s5f$ transition of helium-like Ne IX at 499.37 Å. The wavelength is known with an accuracy ± 0.004 Å by [126,127] and provides a good calibration for our measurements. The standard error for wavelength calibration is 0.02 Å in the region of 490-500 Å. The spectroscopic linewidths are about 0.4 Å. The fitted curve is shown in Fig. 5.1.1(e).

For $1s2s2p^23s\ ^6P_J-1s2p^33s\ ^6S^o$ transitions we also expected to resolve the fine structures in our experiments. The wavelengths for the $J=7/2, 5/2, 3/2-5/2$ transitions are 498.54 ± 0.05 Å, 497.08 ± 0.05 Å and 495.49 ± 0.05 Å. The ratios of the three transition rates are found to be about 7.7:5.9:4.0, and are consistent with the theoretical values of 8:6:4 within experimental error. From the transition rates we verify our identifications of the three transitions. In Table 5.1.1 we present our measured fine structure wavelength values and compare these with our theoretical values for Ne VI. The associated fine structures of the lower state $1s2s2p^23s\ ^6P_J$ for $J=7/2-5/2$ and $J=5/2-3/2$ are $589\pm 15\text{ cm}^{-1}$ and $646\pm 15\text{ cm}^{-1}$ as listed in Table 5.1.2, and are consistent with our calculations.

5.1.4. Comparison of the $1s2s2p^23s\ ^6P-1s2p^33s\ ^6S^o$ Transitions with Theory along Isoelectronic Sequence

In Fig. 5.1.2(a) we show a plot of the center of gravity of the $1s2s2p^23s\ ^6P-1s2p^33s\ ^6S^o$ transition wavelengths $\lambda(Z-3)$ for boron-like ions. The experimental results show good consistency with the trend of the various calculations for $Z=5-13$. Detailed comparisons of the deviations of calculated transition energy from experiment for O IV, F V and Ne VI are shown in Fig. 5.1.2(b). The error bars of the experiments are small and inside the circles. The errorbars of calculated energies are the root mean square differences of calculated transition energy with the same type of calculation method from experiments for the same type of transition along the isoelectronic sequence. The errorbars of the SCHF, SCHFT, MCHF, MCHFT, SCDF and MCDF calculations are within ± 188 , ± 107 , ± 549 , ± 531 , ± 4172 and $\pm 629\text{ cm}^{-1}$, respectively. Thus, we can see i) the single configuration interaction is the most important main part of the all configuration interactions, ii) the interactions between the configurations that we chose are effective to get more accurate results, and iii) the sextet transition energies are sensitive to both relativistic and electron correlation effects.

In Table 5.1.2 we summarize the detailed results of the fine structures of the $1s2s2p^23s\ ^6P_J$ state for O IV, F V and Ne VI. The comparison of the measured fine structures of the $1s2s2p^23s\ ^6P_J$ state with theoretical values shows reasonable agreement (see Fig. 5.1.3). Here the error bars of experiments are also small and inside the circles.

TABLE 5.1.2. Fine structure (in cm^{-1}) of the $1s2s2p^23s\ ^6P_J$ states in O IV, F V and Ne VI.

Z	Experiment	schft	mchft	scdf	mcdf	Experiment	schft	mchft	scdf	mcdf
	$J=7/2-5/2$					$J=5/2-3/2$				
8	254±19	257	245	224	268	(345±19)	343	246	174	288
				163					211	
9	371±38	486	132	144	246	367±38	408	513	3	325
				367					410	
10	589±15	605	744	765	1161	646±15	760	467	753	841
				655					687	

TABLE 5.1.3. Lifetime (in ps) of the $1s2s2p^23s\ ^6P$ and $1s2p^33s\ ^6S^o_{5/2}$ states in O IV, F V and Ne VI.

Z	This work				Experiment[15]	Others	
	SCHF	MCHF	SCDF	MCDF		MCDF[15]	MCHF[16]
	$1s2s2p^23s\ ^6P$						
8	221.13	118.76	306.39	182.81	99±12	125	140
9	118.46	61.44	159.93	85.93	73±15	64	71.22
10	70.09	42.48	92.07	47.70			
	$1s2p^33s\ ^6S^o_{5/2}$						
8	217.05	231.13	405.00	325.90			
9	185.05	312.29	330.48	269.97			
10	160.90	250.17	278.28	228.17			

TABLE 5.1.4. Electron screening σ for the 2s and 2p valence electron of the $1s2s2p^23s\ ^6P$ and $1s2p^33s\ ^6S^o_{5/2}$ states in O IV, F V and Ne VI.

Z	$1s2s2p^23s\ ^6P_J$				$1s2p^33s\ ^6S^o_{5/2}$		
	SCHF	MCHF	SCDF	MCDF	MCHF	SCHF	MCHF
	J=7/2	J=5/2	J=3/2	AV	AV	J=5/2	J=5/2
8	2.1577	2.1572	2.1565	2.1578	2.1362	2.6520	2.6290
9	2.1554	2.1545	2.1534	2.1535	2.1354	2.6380	2.6197
10	2.1524	2.1524	2.1496	2.1492	2.1357	2.6272	2.6145
AV	2.1552	2.1559	2.1549	2.1535	2.1357	2.6391	2.6211
ER	0.0026	0.0031	0.0035	0.0025	0.0002	0.0718	0.0425

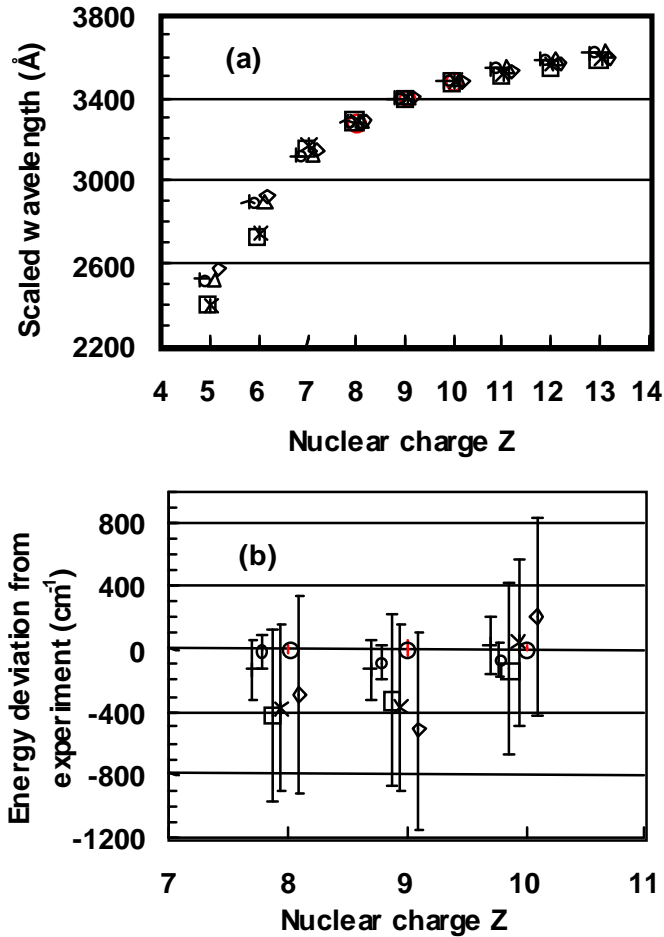


FIG. 5.1.2. Scaled isoelectronic plot of the center of gravity wavelength (a) and transition energy deviations from experiment (b) of the $1s2s2p^2 3s \ ^6P-1s2p^3 3s \ ^6S^o$ multiplet transitions for the Boron sequence. The experimental and calculated points are denoted by the following: circles with error bars inside for experiments, + for SCHF, o for SCHFT, \square for MCHF, * for MCHFT, Δ for SCDF, and diamonds for MCDF.

The QED effects and higher order corrections for the $1s2s2p^2 3s \ ^6P-1s2p^3 3s \ ^6S^o$ transitions in O IV, F V and Ne VI are up to about $1.1-400 \text{ cm}^{-1}$ (see Table 5.1.1) and cannot be ignored in careful comparisons with the experiments. Here the

QED effects and higher order corrections are calculated based on the Z_{eff} 's from the SCHF and MCHF results. We plot the QED effects and higher order corrections to the mean $1s2s2p^23s$ 6P - $1s2p^33s$ ${}^6S^{\circ}$ transition energies in Fig. 5.1.4. The QED effects increase with increasing Z rapidly. The results show the mean transition wavelengths are sensitive to the QED effects of 0.099\AA , 0.129\AA and 0.17\AA for the $1s2s2p^23s$ 6P - $1s2p^33s$ ${}^6S^{\circ}$ transitions in O IV, F V and Ne VI. Thus, they are at the same level or larger than our estimated experimental precision of $\pm 0.10\text{\AA}$, $\pm 0.15\text{\AA}$ and $\pm 0.05\text{\AA}$.

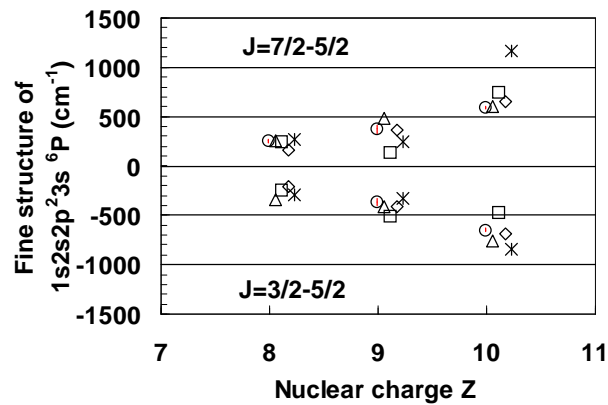


FIG. 5.1.3. Comparison of the experimental (opened circles) and theoretical (others) fine structures for O IV, FV and Ne VI. The experimental and calculated points are denoted by the following: circles with error bars inside for experiments, Δ for SCHFT, \square for MCHFT, diamonds for SCDF, and * for MCDF.

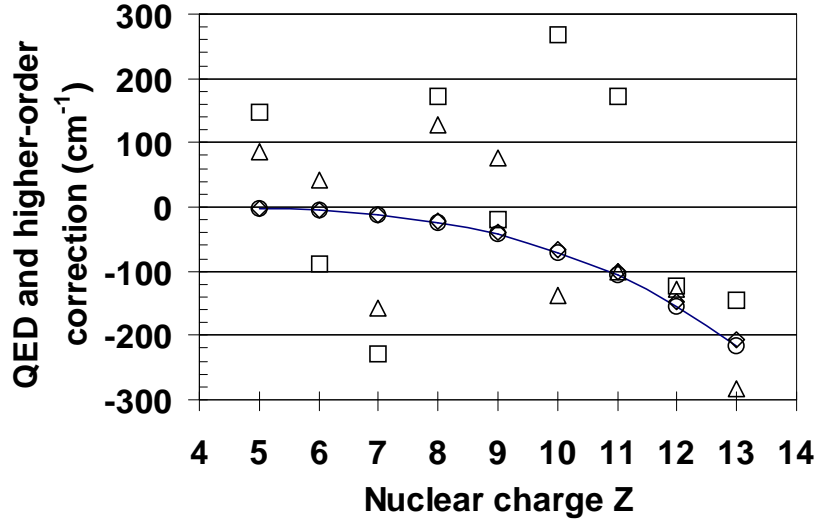


FIG. 5.1.4. Isoelectronic comparison of the QED effects and higher-order corrections of the $1s2s2p^23s\ ^6P-1s2p^33s\ ^6S^o$ transitions for the boron sequence. The calculated points are denoted by the following: diamonds for QED effects from SCHF, Δ for higher order corrections from SCHF, \circ for QED effects from MCHF, and \square for higher order corrections from MCHF. The fitted QED effects from both SCHF and MCHF are denoted by solid line.

Table 5.1.3 shows that our MCHF and MCDF calculated lifetime results for the $1s2s2p^23s\ ^6P$ states for O IV, F V and Ne VI are in fair agreement with the measurements by Blanke et al [15] and the calculations of Blanke [15] and Miecznik et al [16] (see Table 5.1.3). The discrepancy between theory and experiments is most probably due to the additional decay modes of M2, radiative autoionization or some missing configurations which are important for MCHF and MCDF calculations, and possibly also from line-blending. However, the SCHF and SCDF calculated lifetime results for the $1s2s2p^23s\ ^6P$ states for O IV, F V and Ne VI disagree significantly with the measurements of Blanke et al [15] and the calculations of Blanke [15] and Miecznik *et al* [16]. In Table 5.1.3 we

also list our calculated lifetime results for the $1s2p^33s\ ^6S^o$ states for O IV, F V and Ne VI.

Fig. 5.1.5(a) shows a plot of the center of gravity of the $1s2s2p^23s\ ^6P-1s2p^33s\ ^6S^o$ transition energies for boron-like ions vs nuclear charge Z . The diamonds are the weighted values of our different calculations. The solid line is a fit to the theoretical values. The circles are for experiments. The errorbars are less than the circle diameter. The straight-line fit expression is

$$E \text{ (in } 10^3 \text{ cm}^{-1}\text{)} = A_0 + A_1 \cdot Z, \quad (9)$$

where $A_0 = -43.5635 \pm 0.6125$ and $A_1 = 24.5097 \pm 0.0654$.

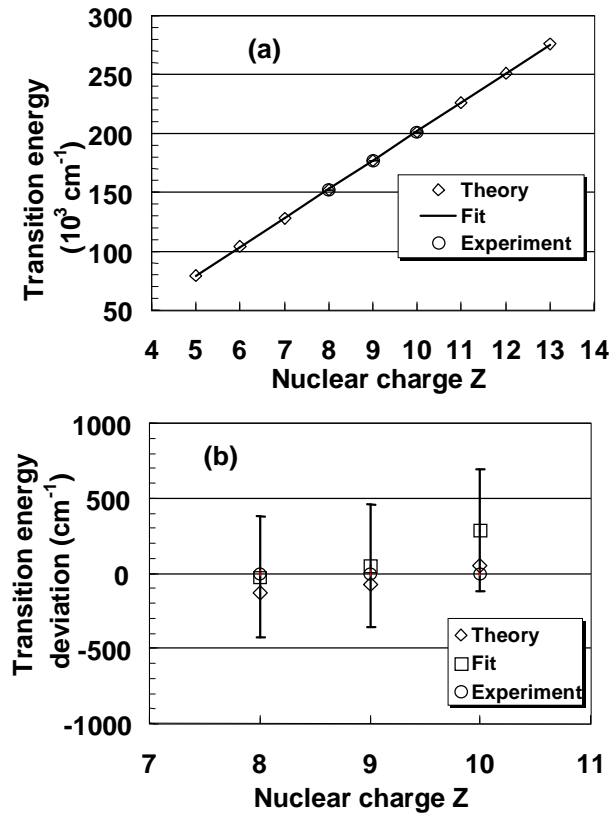


FIG. 5.1.5. Isoelectronic comparison of the theoretical and experimental mean wavelengths of the $1s2s2p^23s\ ^6P-1s2p^33s\ ^6S^o$ transitions for the boron sequence.

Our measured transition energies for O IV, F V and Ne VI are consistent with the trend of our different calculations shown in Fig. 5.1.5(a). The fine structures of the sextet states of the boron-like isoelectronic sequence are very similar, so that the screened hydrogen-like calculation is a good approximation. For the same type of sextet states the electron screening σ almost does not change with the nuclear charge Z (see Table 5.1.4). With $Z_{\text{eff}} = Z - \sigma$, the transition energy can be written as

$$\begin{aligned} \Delta E &\sim -\frac{Z_{\text{eff upper}}^2}{2^2} + \frac{Z_{\text{eff lower}}^2}{2^2} \sim -\frac{1}{4} [(Z - \sigma_{\text{up}})^2 + (Z - \sigma_{\text{lo}})^2] \\ &\sim \frac{1}{4} (\sigma_{\text{up}} - \sigma_{\text{lo}})[2Z - (\sigma_{\text{up}} + \sigma_{\text{lo}})], \end{aligned} \quad (10)$$

leading to the linear relation. In order to see more detail Fig. 5.1.6(b) shows the deviations of the calculated (marked as diamonds) and the fitted (marked as squares) transition energies from the experiments for O IV, F V and Ne VI. They are less than 300 cm^{-1} . Hence, the equations (9) and (10) provide accurate energy approximations of the $1s2s2p^23s \ ^6P - 1s2p^33s \ ^6S^o$ transitions in boron-like ions for $Z=5$ to 13.

5.1.5. Summary

The wavelengths and fine structures for $1s2s2p^23s \ ^6P_J - 1s2p^33s \ ^6S^o$ transitions in O IV, F V, and Ne VI have been investigated by beam foil spectroscopy and compared with the theoretical values obtained using the MCHF plus higher order contributions and QED effect numerical calculations, and with the MCDF method. We have carefully studied the effect of configuration interaction, higher-order corrections and QED effect on the energies, and relevant E1 transition energies and wavelengths. Agreement for the energies of the doubly

excited sextet states $1s2s2p^23s\ ^6P_J$ and $1s2p^33s\ ^6S^0$ and their fine structures is satisfactory. We have also studied the effect of the configuration interaction on the transition probabilities and lifetimes. For the lifetimes for the $1s2s2p^23s\ ^6P$ states in O IV and F V there remains large discrepancies of about 20% between our MCHF and MCDF calculations and experiments [15].

5.2 The $1s2s2p^23p\ ^6L^o-1s2p^33p\ ^6P$, L=S, P, D Transitions in O IV, F V and Ne VI

In the section we present observations of VUV transitions between doubly excited sextet states of O IV. Spectra were produced by collisions of O⁺ beam with a solid carbon target. We also studied the spectra obtained previously of F V and Ne VI. Some observed lines were assigned to the $1s2s2p^23p\ ^6L-1s2p^33p\ ^6P$, L=S, P, D, electric-dipole transitions and are in good agreement with our accurate MCHF (with QED and higher-order corrections) and MCDF calculations. 31 new lines have been identified.

Fig. 5.2.1(a) -(c) display three typical spectra of oxygen at the beam energy 1.5, 1.7 and 2.5 MeV in the wavelength range 660-710 Å. Fig. 5.2.1(d) and (e) display the spectra of $^{20}\text{(FH)}^+$ and $^{20}\text{Ne}^+$ at the beam energy 2.5 and 4.0 MeV in the wavelength range 560-640 Å and 490-540 Å. The sextet transitions appear as weak lines among a rich collection of other sometimes unidentified lines of highly excited oxygen, fluorine and neon. The peak location vs. dial was found using non-linear least squared fits to Gaussian profiles first. The wavelength determining procedures and results are described below.

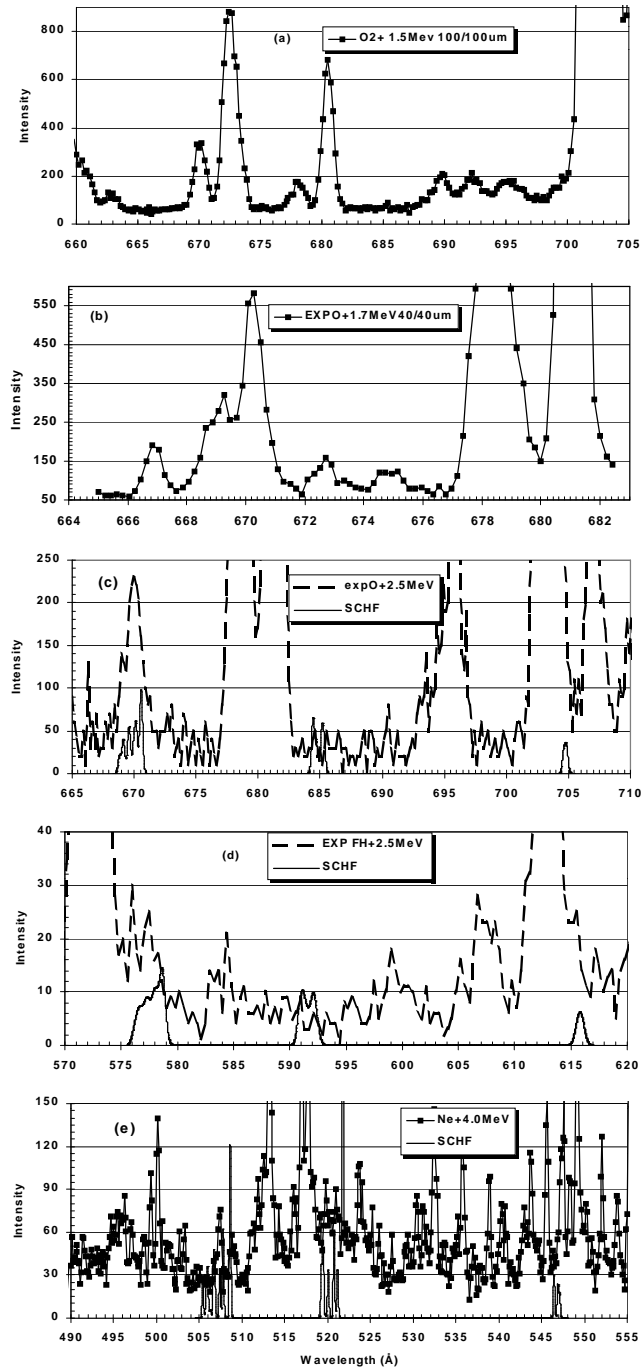


FIG. 5.2.1. The $1s2s2p^23p \ ^6L$ and $1s2p^33p \ ^6P$ transitions in the beam-foil spectra of oxygen, fluorine and neon, recorded at the different energies. The beam energies and spectrometer slit widths are indicated.

5.2.1 The $1s2s2p^23p\ ^6L^o-1s2p^33p\ ^6P$ Transitions in O IV.

In the wavelength region where the transitions between the sextet states $1s2s2p^23p\ ^6L$ and $1s2p^33p\ ^6P$ in O IV were expected we obtained several spectra at different ion beam energies for oxygen. Three typical spectra are shown in Fig. 5.2.1(a) -(c). For the $1s2s2p^23p\ ^6L-1s2p^33p\ ^6P$ transitions we expected to partially resolve the fine structures of the lower states $1s2s2p^23p\ ^6L$ in our experiments, whereas the fine structures of the upper states $1s2p^33p\ ^6P$ are too close and less than the resolution of the experimental spectra. A promising candidate for the $1s2s2p^23p\ ^6D_{9/2} - 1s2p^33p\ ^6P_{7/2}$ transitions at $668.95\pm 0.08\ \text{\AA}$ appears at the 1.7 and 2.5 MeV O^+ ion beam energy, which does not appear in the spectrum of the 1.2 MeV O_2^+ ion beam energy. The well-known transitions of O V 3p-4d, O IV $2s^23p-2s^25s$, O V 2s3d-2s4f and O III $2s^22p^2-2s2p^3$ are at 659.589 \AA , 670.601 \AA , 681.332 \AA and 703.854 \AA respectively, close to the doubly excited sextet transitions in the neighborhood. The wavelengths have been semiempirically fitted with high accuracy of $\pm 0.004\ \text{\AA}$ by [134-136] and provided a good calibration for our measurements. The standard error for wavelength calibration is 0.01 \AA in the region of 660-710 \AA . Nonlinear least square fits of Gaussian profiles give the values for the wavelengths, intensities and full widths at half maximum (FWHM) of lines. The uncertainties of the wavelengths are related to the intensities of the lines. Through the use of optical refocusing we achieved spectroscopic linewidths of 0.7 \AA . The precision of the profile-fitting program was checked through several known transition wavelengths.

In Table 5.2.1 all the observed lines in the sextet system of O IV are reported. Nine lines are new observations with the wavelength accuracy of $\pm 0.06 \text{ \AA}$. Most of the new identifications have been obtained by searching in our spectra for sets of unidentified lines and by comparing the energies and relative intensities in agreement with our accurate MCHF and MCDF theoretical predictions. The transition rate is proportional to the area of the peak (the fitted intensity \times FWHM of the experiments).

The strongest transition related to individual fine structure components is the $1s2s2p^23p \text{ } ^6D_{9/2} - 1s2p^33p \text{ } ^6P_{7/2}$ transition at the wavelength of $668.95 \pm 0.08 \text{ \AA}$. We also got the wavelength for the $1s2s2p^23p \text{ } ^6D_J - 1s2p^33p \text{ } ^6P_J$ transition. The transition rate is proportional to the area of the peak. We compared the measured transition rates with calculated results. Fig. 5.2.2(a) and (b) display the identifications of the $1s2s2p^23p \text{ } ^6D_J - 1s2p^33p \text{ } ^6P_J$ and $1s2s2p^23p \text{ } ^6S_{5/2} - 1s2p^33p \text{ } ^6P_J$ transitions of O IV in the experimental spectrum of oxygen at the energy of 2.5 MeV.

In Table 5.2.1 we present our measured fine structure wavelength values and compare these with our various theoretical values for O IV. Our experiments are consistent with our calculations.

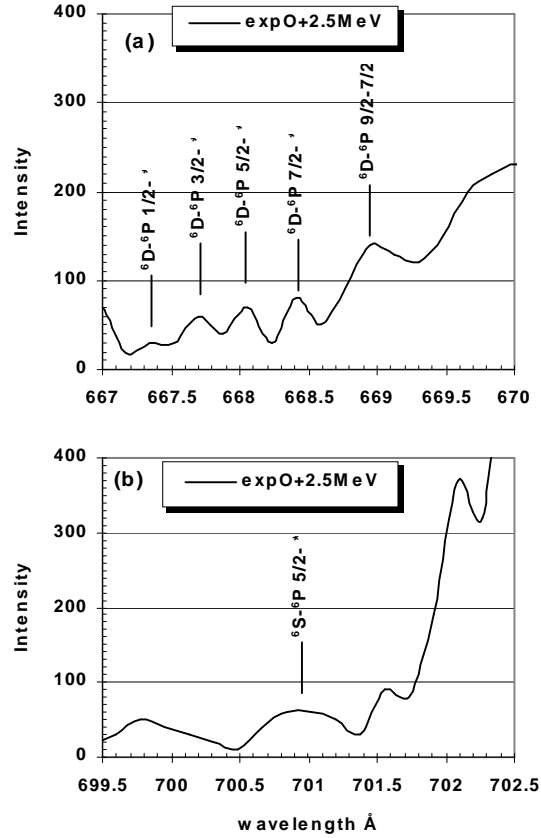


FIG. 5.2.2. The identifications of the $1s2s2p^23p\ ^6D_J - 1s2p^33p\ ^6P_J$ and $1s2s2p^23p\ ^6S_{5/2} - 1s2p^33p\ ^6P_J$ transitions of O IV in the experimental spectrum of O at the energy of 2.5 MeV. In (a) * means all possible J's of the upper states allowed by E1 transition rules. In (b) * means 3/2, 5/2 and 7/2.

5.2.2 The $1s2s2p^23p\ ^6L^o - 1s2p^33p\ ^6P$ Transitions in F V.

We obtained spectra at a beam energies of 2.5 MeV for fluorine. In the wavelength region the transitions between the sextet states $1s2s2p^23p\ ^6L$ and $1s2p^33p\ ^6P$ in F V were expected. The spectrum in the wavelength region of 570-620 Å is shown in Fig. 5.2.1(d). A promising candidate for the $1s2s2p^23p\ ^6D_{9/2} - 1s2p^33p\ ^6P_{7/2}$ transitions at 577.50 ± 0.10 Å appears in the spectrum of the 2.5

MeV (FH)⁺ ion beam energy. Using similar experimental analysis procedure described above, we obtained the wavelength accuracy of ± 0.10 Å for the $1s2s2p^23p$ ⁶L - $1s2p^33p$ ⁶P transitions in the wavelength region of 570-620 Å.

In Table 5.2.1 all the observed lines in the sextet system of F V are reported. Nine lines are new observations. Most of the new identifications have been obtained by searching in our spectra for sets of unidentified lines and by comparing the energies and relative intensities in agreement with our accurate MCHF and MCDF theoretical predictions.

The strongest fine structure component is the $1s2s2p^23p$ ⁶D_{9/2} - $1s2p^33p$ ⁶P_{7/2} transition at the wavelength of 577.50 ± 0.10 Å. We also found the wavelength for the $1s2s2p^23p$ ⁶D_J - $1s2p^33p$ ⁶P_J transitions. The transition rates are proportional to the area of the peaks and our measured transition rates compare well with our calculated results. In Table 5.2.1 we present our measured fine structure wavelength values and compare these with our various theoretical values for F V. The two sets of results are consistent.

5.2.3 The $1s2s2p^23p$ ⁶L^o - $1s2p^33p$ ⁶P Transitions in Ne VI.

We obtained spectra at a beam energies of 4.0 MeV for Neon. In the wavelength region the transitions between the sextet states $1s2s2p^23p$ ⁶L and $1s2p^33p$ ⁶P in Ne VI were expected. The spectrum in the wavelength region of 490-550 Å is shown in Fig. 5.2.1(e). A promising candidate for the $1s2s2p^23p$ ⁶D_{9/2} - $1s2p^33p$ ⁶P_{7/2} transition at 507.13 ± 0.05 Å appears at the 4.0 MeV Ne⁺ ion beam energy. Nonlinear least square fits of Gaussian profiles give the values for the wavelengths, intensities and full widths at half maximum (FWHM) of lines. The uncertainties of the wavelengths are related to the intensities of the lines. Through the use of optical refocusing we achieved spectroscopic linewidths of 0.4 Å in the second order spectrum. The precision of the profile-fitting program

was also checked through the known transition wavelengths. Using the similar experimental procedure we obtained the wavelength accuracy of $\pm 0.05 \text{ \AA}$ for the $1s2s2p^23p \text{ } ^6L - 1s2p^33p \text{ } ^6P$ transitions in the wavelength region of 570-620 \AA .

In Table 5.2.1 all the observed lines in the sextet system of Ne VI are reported. Nine lines are new observations with the wavelength accuracy of $\pm 0.05 \text{ \AA}$.

The strongest transition related to fine structure component is the $1s2s2p^23p \text{ } ^6D_{9/2} - 1s2p^33p \text{ } ^6P_{7/2}$ transition at the wavelength of $507.13 \pm 0.05 \text{ \AA}$. We compared the measured transition rates with calculated results. They are consistent. In Table 5.2.1 we present our measured fine structure wavelength values and compare these with our various theoretical values for Ne VI.

5.2.4 Comparison of the $1s2s2p^23p \text{ } ^6L^o - 1s2p^33p \text{ } ^6P$ Transitions with Theory along Isoelectronic Sequence

In order to verify the validity of our experimental and theoretical approaches above, we have studied the deviations between the experimental and theoretical transition energies of the $1s2s2p^23p \text{ } ^6L^o - 1s2p^33p \text{ } ^6P$ transitions along the boron-like isoelectronic sequence. In Figs. 5.2.3, 4 and 5 we show plots of the deviations between the experimental and theoretical transition energies of the $1s2s2p^23p \text{ } ^6D^o$, P^o and $S^o - 1s2p^33p \text{ } ^6P$ transitions for boron-like ions.

In Fig. 5.2.3 we can see the SCHF and SCDF deviations are constant for all $1s2s2p^23p \text{ } ^6D^o - 1s2p^33p \text{ } ^6P$ transitions of nuclear charge with $Z = 8, 9$ and 10 . The MCDF and non-relativistic SCHF deviations are linear for all $1s2s2p^23p \text{ } ^6D^o - 1s2p^33p \text{ } ^6P$ transitions of nuclear charge with $Z = 8, 9$ and 10 . The MCHF deviation of oxygen is very small, 22 cm^{-1} .

TABLE 5.2.1. The energies E (in cm^{-1}) and wavelengths λ (in \AA) for the $1s2s2p^23p\ ^6L_J-1s2p^33p\ ^6P_J$ transitions in O IV, F V and Ne VI by this work. We also list the deviations between the theoretical and experimental transition energies for the $1s2s2p^23p\ ^6L_J-1s2p^33p\ ^6P_J$ transitions.

Ions	λ exp	Eexp	λ mchf	Emchf	dEcal	λ schf	E schf	dEcal	λ scdf	Escdf	dEcal	λ mcdf	Emcdf	dEcal
J-J'														
O IV	± 0.06													
<i>1s2s2p²3p⁶D_J-1s2p³3p⁶P_J</i>														
				± 32			± 372		± 710			± 1938		
1/2-*	667.26	149867	667.36	149844	-22	668.82	149517	-350	664.15	150568	702	658.84	151782	1915
3/2-*	667.70	149768	667.68	149772	4	669.12	149450	-318	664.58	150471	703	659.12	151717	1950
5/2-*	668.04	149692	668.13	149671	-20	669.59	149345	-347	665.00	150376	684	659.59	151609	1918
7/2-*	668.41	149609	668.54	149580	-29	670.10	149231	-377	665.64	150231	623	660.11	151490	1881
9/2-7/2	668.95	149488	669.07	149461	-27	670.57	149127	-361	666.27	150089	601	660.62	151373	1885
AVwei	668.34	149623	668.44	149602	-22	669.94	149267	-356	665.48	150267	644	660.66	151364	1740
AVunw	668.07	149684	668.16	149666	-19	669.64	149334	-350	665.13	150347	663	659.66	151594	1910
QED				-23.6			-23.4							
HO				139.6			-16.7							
AVwei ^T			667.92	149718	95	670.12	149227	-396						
nonrel						673.61	148453	-1170						
<i>1s2s2p²3p⁶P_J-1s2p³3p⁶P_J</i>														
				± 258			± 555		± 1782			± 677		
3/2-*	687.14	145531	685.94	145785	255	684.51	146090	559	678.94	147288	1758	676	147951	676
5/2-*	687.35	145486	686.23	145724	237	685.04	145977	491	679.15	147243	1757	676	147890	676
7/2-*	687.65	145423	686.69	145626	203	685.25	145932	509	679.91	147078	1655	677	147763	677
AVwei	687.44	145468	686.37	145694	226	685.02	145982	514	679.44	147180	1712	676.38	147847	676
AVunw	687.38	145480	686.29	145712	232	684.93	146000	520	679.33	147203	1723	676.28	147868	676
QED				-23.5			-23.3							
HO				29.1			-39.1							
AVwei ^T			686.34	145700	232	685.31	145920	452						
nonrel						688.66	145209	-259						
<i>1s2s2p²3p⁶S_J-1s2p³3p⁶P_J</i>														
				± 7507			± 771		± 4252			± 5880		
5/2-*	700.93	142668	739.86	135161	-7507	704.74	141896	-771	722.46	138416	-4252	731.06	136788	-5880
QED				-23.0			-23.1							
HO				149.3			66.7							
AVwei ^T			739.17	135287	-7381	704.53	141940	-728						
nonrel						708.76	141091	-1576						

TABLE 5.2.1. Continued.

Ions	λ exp	Eexp	λ mchf	Emchf	dEcal	λ schf	E schf	dEcal	λ mcdmf	Emcdmf	dEcal	λ scdf	Escdf	dEcal
J-J'														
F V	± 0.10													
<i>1s2s2p²3p ⁶D_J-1s2p³3p ⁶P_J</i>														
				± 1043			± 328		± 965			± 2767		
1/2-3/2	575.20	173853	572.17	174773	921	576.24	173539	-314	572.33	174724	872	566.42	176547	2695
3/2-*	575.85	173656	572.40	174703	1047	576.61	173427	-229	572.72	174605	949	566.77	176438	2782
5/2-*	576.43	173482	573.26	174441	959	577.23	173241	-240	573.30	174429	947	567.46	176224	2742
7/2-*	577.09	173283	573.89	174249	966	577.95	173025	-258	574.15	174171	887	568.49	175905	2621
9/2-7/2	577.50	173160	574.04	174204	1044	578.66	172813	-347	575.06	173895	735	569.01	175744	2584
AVwei	576.80	173369	573.50	174368	998	577.75	173085	-284	573.97	174225	855	568.09	176028	2659
AVunw	576.41	173486	573.15	174474	987	577.34	173209	-278	573.51	174364	878	567.63	176171	2685
QED				-41.7			-41.4							
HO				211			372.5							
AVwei ^T			572.94	174537	1168	576.65	173416	47						
nonrel						582.31	171729	-1640						
<i>1s2s2p²3p ⁶P_J-1s2p³3p ⁶P_J</i>														
				± 1084			± 418		± 1761			± 2783		
3/2-*	592.45	168791	589.86	169532	741	591.01	169202	411	587.55	170198	1408	582.83	171577	2786
5/2-*	592.67	168728	589.13	169742	1014	591.26	169130	402	586.65	170459	1731	583.17	171477	2749
7/2-*	593.43	168512	589.86	169532	1020	592.16	168873	361	587.70	170155	1643	583.96	171245	2733
AVwei	592.96	168646	589.62	169602	956	591.60	169032	386	587.32	170266	1620	583.45	171396	2750
AVunw	592.85	168677	589.62	169602	925	591.48	169068	392	587.30	170271	1594	583.32	171432	2756
QED				-41.5			-41.2							
HO				216.2			343.4							
AVwei ^T			589.01	169777	1131	590.55	169334	688						
nonrel						596.37	167682	-964						
<i>1s2s2p²3p ⁶S_J-1s2p³3p ⁶P_J</i>														
				± 6116			± 105		± 4428			± 5379		
5/2-*	615.57	162451	639.65	156335	-6116	615.97	162346	-105	632.82	158023	-4428	636.65	157072	-5379
QED				-40.7			-40.8							
HO				251.1			176.5							
AVwei ^T			638.79	156545	-5906	615.45	162482	31						
nonrel						620.9	161058	-1393						

TABLE 5.2.1. Continued.

Ions	λ exp	Eexp	λ mchf	Emchf	dEcal	λ schf	E schf	dEcal	λ mcdmf	Emcdf	dEcal	λ scdf	Escdf	dEcal
J-J'	± 0.05													
Ne VI														
<i>1s2s2p²3p ⁶D_J-1s2p³3p ⁶P_J</i>														
				± 917			± 557		± 1153			± 3492		
1/2-3/2	505.20	197941	502.64	198950	1008	505.41	197859	-82	502.07	199175	1234	496.29	201495	3554
3/2-*	505.44	197847	503.19	198732	885	505.96	197644	-203	502.50	199005	1158	496.62	201361	3514
5/2-	505.77	197718	503.87	198464	746	506.72	197348	-371	503.40	198649	931	497.52	200997	3279
3/2,5/2														
7/2-7/2	506.17	197562	504.55	198196	634	507.39	197087	-475	504.20	198334	772	498.26	200698	3136
7/2-5/2	506.50	197433	504.96	198035	602	507.78	196936	-498	504.53	198204	771	498.67	200533	3100
9/2-7/2	507.13	197188	505.78	197714	526	508.61	196614	-574	505.47	197836	648	499.53	200188	3000
AVwei	506.29	197517	504.56	198192	675	507.38	197089	-428	504.13	198361	844	498.23	200710	3193
AVunw	506.04	197615	504.17	198348	733	506.98	197247	-368	503.70	198533	918	497.82	200878	3263
QED				-68.2			-66.8							
HO				-220.0			78.9							
AVwei ^T			505.30	197904	387	507.35	197101	-416						
nonrel						512.88	194977	-2540						
<i>1s2s2p²3p ⁶P_J-1s2p³3p ⁶P_J</i>														
				± 1190			± 119		± 1832			± 3013		
3/2-5/2	519.53	192482	516.38	193656	1174	519.23	192593	111	514.98	194182	1701	511.58	195473	2991
5/2-7/2,	519.77	192393	516.55	193592	1199	519.46	192508	115	515.21	194096	1703	511.73	195416	3023
3/2-3/2														
5/2-3/2	520.26	192212	517.20	193349	1137	520.06	192286	74	516.00	193798	1587	512.32	195191	2979
7/2-7/2	520.78	192020	517.81	193121	1101	520.74	192034	15	515.64	193934	1914	512.93	194958	2939
7/2-5/2	521.36	191806	518.24	192961	1155	521.15	191883	77	517.02	193416	1610	513.38	194787	2981
Avwei	520.35	192178	517.24	193333	1156	520.14	192255	77	515.72	193903	1726	512.39	195162	2984
Avunw	520.54	192107	516.99	193429	1322	520.35	192177	70	515.97	193811	1703	512.59	195088	2980
QED				-67.8			-66.5							
HO				-50.3			-10.7							
AVwei ^T			517.56	193215	1037	520.35	192178	0						
Nonrel						525.74	190137	-2041						
<i>1s2s2p²3p ⁶S_J-1s2p³3p ⁶P_J</i>														
				± 5314			± 735		± 4341			± 4617		
5/2-7/2	548.62	182276	564.89	177026	-5250	546.46	182996	720	561.94	177955	-4321	562.5	177778	-4498
5/2-	548.94	182169	565.40	176866	-5303	546.99	182819	649	562.33	177832	-4338	563.15	177573	-4597
5/2,3/2														
Avwei	548.80	182216	565.17	176937	-5280	546.75	182897	681	562.16	177886	-4330	562.86	177664	-4553
Avunw	548.78	182222	565.15	176946	-5277	546.73	182907	685	562.14	177893	-4329	562.83	177675	-4547
QED				-66.7			-66.7							
HO				-165.6			16.5							
AVwei ^T			565.92	176705	-5511	546.91	182847	631						
Nonrel						553.04	180817	-1459						

In Fig. 5.2.4 the SCDF deviation is constant for all $1s2s2p^23p\ ^6P^o - 1s2p^33p\ ^6P$ transitions of nuclear charge with $Z = 8, 9$ and 10 . The MCHF, SCHF, MCDF and non-relativistic SCHF deviations are linear for all $1s2s2p^23p\ ^6P^o - 1s2p^33p\ ^6P$ transitions of nuclear charge with $Z = 8, 9$ and 10 . The MCHF deviation of oxygen is 226 cm^{-1} . In Fig. 5.2.5 we can see the SCDF and relativistic SCHF deviations are constant for all $1s2s2p^23p\ ^6S^o - 1s2p^33p\ ^6P$ transitions of nuclear charge with $Z = 8, 9$ and 10 . The MCHF, MCDF and SCHF deviations are linear for all $1s2s2p^23p\ ^6S^o - 1s2p^33p\ ^6P$ transitions of nuclear charge with $Z = 8, 9$ and 10 . The SCHF deviation of oxygen is 105 cm^{-1} . But the SCDF, MCHF and SCDF deviations are quite large, $>4000\text{ cm}^{-1}$ for all $1s2s2p^23p\ ^6S^o - 1s2p^33p\ ^6P$ transitions of nuclear charge with $Z = 8, 9$ and 10 . To begin with, these above linear or constant energy deviations can be used to predict easily and with high accuracy the transition energies for the $1s2s2p^23p\ ^6D^o, P^o$ and $S^o - 1s2p^33p\ ^6P$ transitions for boron-like ions with the $5 < Z < 13$.

The QED and higher-order corrections for the $1s2s2p^23p\ ^6D^o, P^o$ and $S^o - 1s2p^33p\ ^6P$ transitions in O IV, F V and Ne VI are up to $-220-370\text{ cm}^{-1}$ (see Table 5.2.1) and can't be ignored in the careful comparisons with experiments. Here the QED and higher-order corrections were calculated from the effective nuclear charge Z_{eff} obtained from the MCHF and SCHF calculations. In Fig. 5.2.6 we plot the above corrections. The results show that the weighted mean wavelengths for the $1s2s2p^23p\ ^6D^o, P^o$ and $S^o - 1s2p^33p\ ^6P$ transitions in O IV, F V and Ne VI are sensitive to the QED and higher-order corrections to 0.18 \AA , 0.12 \AA and 0.22 \AA , respectively. They are larger than our estimated experimental precision of $\pm 0.06\text{ \AA}$, $\pm 0.10\text{ \AA}$ and $\pm 0.05\text{ \AA}$.

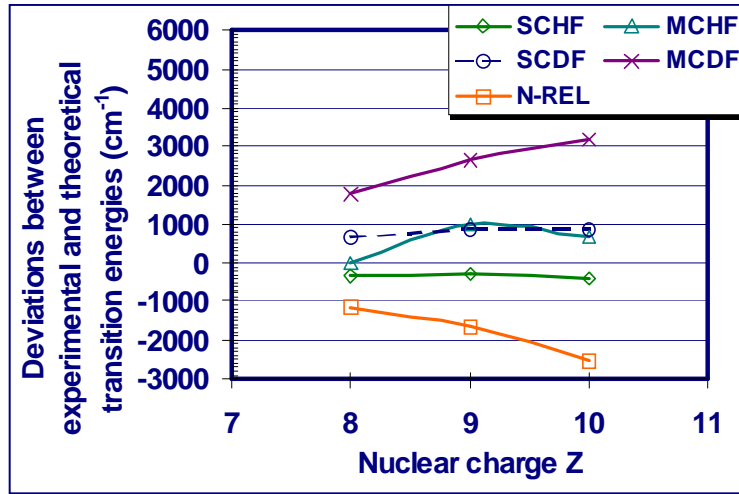


FIG. 5.2.3. The deviations between the theoretical and experimental transition energies for the $1s2s2p^2 3p \ ^6D_J-1s2p^3 3p \ ^6P_J$ transitions. Here the theoretical transition energy is the center of gravity of the $1s2s2p^2 3p \ ^6D_J-1s2p^3 3p \ ^6P_J$ transition energies (computed from the fine structure lines by this work) with the results of theoretical analysis, and the experimental transition energy is the center of gravity of the $1s2s2p^2 3p \ ^6D_J-1s2p^3 3p \ ^6P_J$ transition energies (computed from the observed lines) with the results of theoretical analysis.

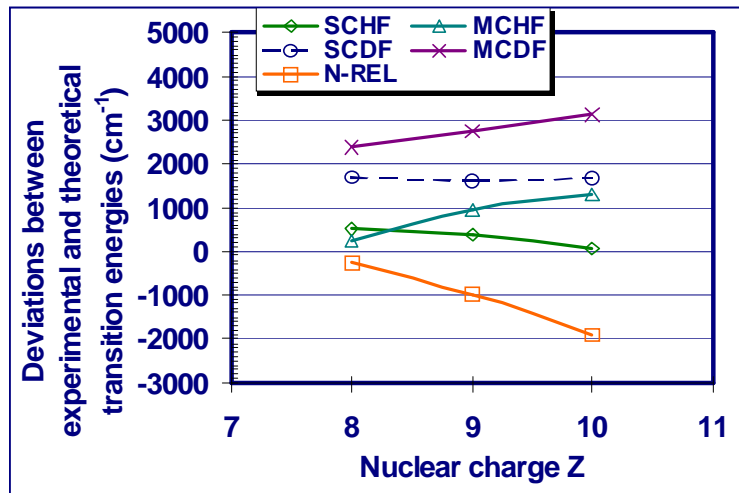


FIG. 5.2.4. The deviations between the theoretical and experimental transition energies for the $1s2s2p^2 3p \ ^6P_J-1s2p^3 3p \ ^6P_J$ transitions. Here the theoretical transition energy is the center of gravity of the $1s2s2p^2 3p \ ^6P_J-1s2p^3 3p \ ^6P_J$ transition energies (computed from the fine structure lines by this work) with the results of theoretical analysis, and the experimental transition energy is the center of gravity of the $1s2s2p^2 3p \ ^6P_J-1s2p^3 3p \ ^6P_J$ transition energies (computed from the observed lines) with the results of theoretical analysis.

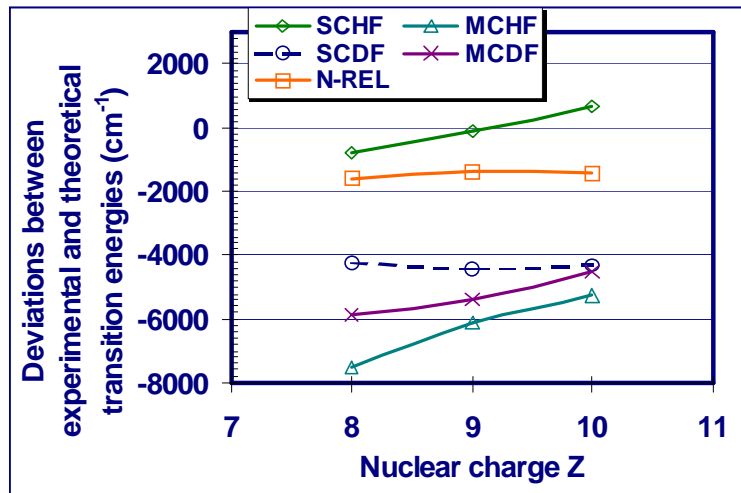


FIG. 5.2.5. The deviations between the theoretical and experimental transition energies for the $1s2s2p^2 3p^6 S_J-1s2p^3 3p^6 P_J$ transitions. Here the theoretical transition energy is the center of gravity of the $1s2s2p^2 3p^6 S_J-1s2p^3 3p^6 P_J$ transition energies (computed from the fine structure lines by this work) with the results of theoretical analysis, and the experimental transition energy is the center of gravity of the $1s2s2p^2 3p^6 S_J-1s2p^3 3p^6 P_J$ transition energies (computed from the observed lines) with the results of theoretical analysis.

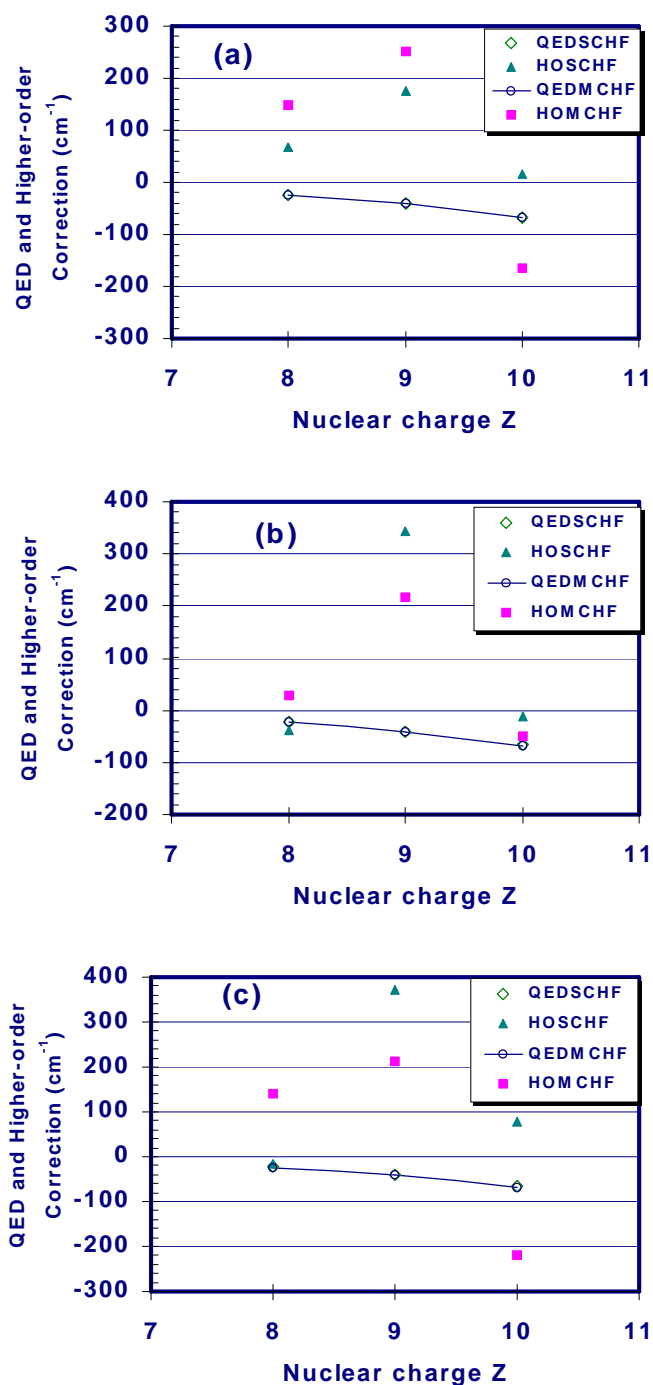


FIG. 5.2.6. The QED and higher-order corrections for (a) the $1s2s2p^23p \ ^6D-1s2p^33p \ ^6P$, (b) $1s2s2p^23p \ ^6P-1s2p^33p \ ^6P$ and (c) $1s2s2p^23p \ ^6S-1s2p^33p \ ^6P$ transitions in the B I isoelectronic sequence.

5.2.5. Summary

Our fast beam-foil spectroscopy experiments have yielded new information on doubly excited sextet states in boron-like O IV. We performed MCHF (with QED and higher-order correction) and MCDF calculations for 2s-2p transitions between doubly excited sextet states of five-electron O IV. Using the calculated wavelengths and transition rates we were able to identify the observed lines in the fast beam-foil spectra for O IV corresponding to the $1s2s2p^23p$ 6L - $1s2p^33p$ 6P , L=S, P, D, electric-dipole transitions in O IV and measure the wavelengths with good accuracy. Most of the new identifications have been obtained by searching in our spectra for sets of unidentified lines and by comparing the energies and relative intensities with our accurate MCHF and MCDF theoretical predictions. Identifications are verified mainly due to the fact that the theoretical transition energy deviation from the experiments is in the reasonable range.

We have carefully studied the effect of the configuration interaction, higher-order corrections and QED effects on the energies, lifetimes and relevant E1 transitions. Agreement for the energies of the doubly excited sextet states $1s2s2p^23p$ ${}^6L^o$ and $1s2p^33p$ 6P and the fine structure of the doubly excited sextet states $1s2s2p^23p$ ${}^6L^o$ is satisfactory. We also have studied the effect of the configuration interaction on the transition probabilities and lifetimes.

5.3 The $1s2s2p^23d\ ^6L - 1s2p^33d\ ^6D^o$, $L=P, D, F$ Transitions in O IV, F V and Ne VI

We present observations of VUV transitions between doubly excited sextet states of O IV, F V and Ne VI. Spectra were produced by collisions of an O⁺ beam with a solid carbon target. Some observed lines were assigned to the $1s2s2p^23d\ ^6L - 1s2p^33d\ ^6D$, $L= P, D, F$ electric-dipole transitions, and are in good agreement with our accurate MCHF (with QED and higher-order corrections) and MCDF calculations. 42 new lines have been identified.

Figs. 5.3.1(a) -(c) display three typical spectra of oxygen recorded at the beam energy 1.5, 1.7 and 2.5 MeV in the wavelength range of 660-710 Å. Figs. 5.3.1(d) and (e) display the spectra of $^{20}(\text{FH})^+$ and $^{20}\text{Ne}^+$ recorded at the beam energy 2.5 and 4.0 MeV in the wavelength range of 560-640 Å and 490-540 Å. The sextet transitions appear as weak lines among a rich collection of other unidentified lines of highly excited oxygen, fluorine and neon. The peak locations vs. dial were found using non-linear least squared fits to Gaussian profiles first. The wavelength determining procedures and results will be described below.

5.3.1 The $1s2s2p^23d\ ^6L - 1s2p^33d\ ^6D^o$ Transitions in O IV.

We obtained spectra at different ion beam energies for oxygen. In the wavelength region of 660-710 Å the transitions between the sextet states $1s2s2p^23d\ ^6L$ and $1s2p^33d\ ^6D$ in O IV were expected. Three typical spectra are shown in Figs. 1(a) -(c). For the $1s2s2p^23d\ ^6L - 1s2p^33d\ ^6D$ transitions we expected to resolve the fine structures of the lower states $1s2s2p^23d\ ^6L$ in our

experiments, whereas the fine structures of the upper states $1s2p^33d\ ^6P$ are too close and less than the resolution of the experimental spectra. A promising candidate for the $1s2s2p^23d\ ^6F_{11/2} - 1s2p^33d\ ^6D_{9/2}$ transition at $666.99\pm0.06\ \text{\AA}$ appears in the spectra recorded at the 1.7 and 2.5 MeV $^{20}\text{O}^+$ ion beam energy, which does not appear in the spectrum at the lower energy of the 1.2 MeV O_2^+ ion beam energy. The O V $3p-4d$, O IV $2s^23p-2s^25s$, O V $2s3d-2s4f$ and O III $2s^22p^2-2s2p^3$ transitions are at $659.589\ \text{\AA}$, $670.601\ \text{\AA}$, $681.332\ \text{\AA}$ and $703.854\ \text{\AA}$, respectively, close to the neighborhood of the doubly excited sextet transitions. The four wavelengths have been semiempirically fitted with high accuracy $\pm0.004\ \text{\AA}$ by [134-136] and provide a good calibration for our measurements. The standard error for wavelength calibration is $0.01\ \text{\AA}$ in the region of 660-710 \AA . Nonlinear least square fits of Gaussian profiles gave the values for the wavelengths, intensities and full widths at half maximum (FWHM) of lines. The uncertainties of the wavelengths are related to the intensities of the lines. Through the use of optical refocusing we achieved spectroscopic linewidths of $0.7\ \text{\AA}$. The precision of the profile-fitting program was checked through several known transition wavelengths.

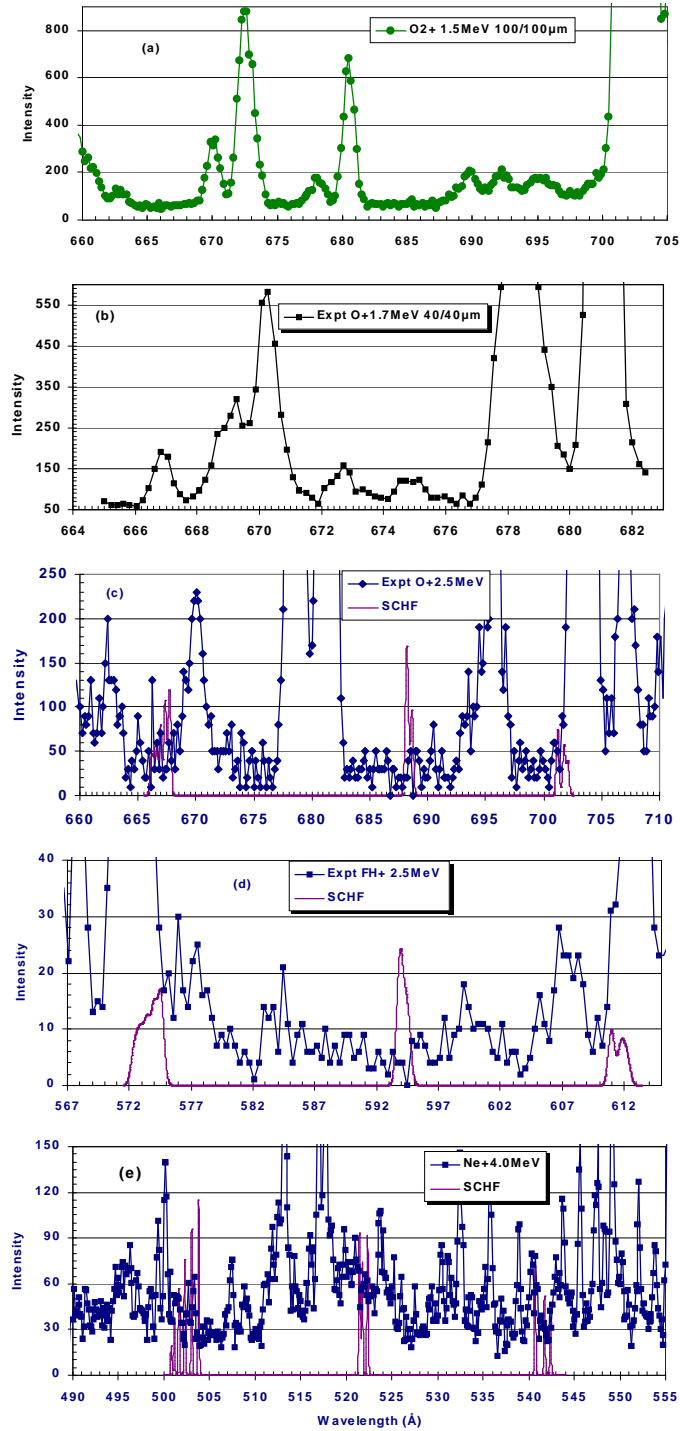


FIG. 5.3.1. The $1s2s2p^23d\ ^6L_J - 1s2p^33d\ ^6D_J$, $L=P, D, F$ transitions in the beam-foil spectra of oxygen, fluorine and neon, recorded at different energies. The beam energies and spectrometer slit widths in are indicated.

Table 5.3.1. The energies E (in cm^{-1}) and wavelengths λ (in \AA) for the $1s2s2p^23d\ ^6L_J-1s2p^33d\ ^6D_J$ transitions in O IV by this work. We also list the deviations between the theoretical and experimental transition energies for the $1s2s2p^23d\ ^6L_J-1s2p^33d\ ^6D_J$ transitions.

J-J'	λ exp ± 0.06	Eexp	λ mchf	Emchf	dEcal	λ schf	E schf	dEcal	λ sCDF	Escdf	dEcal	λ mcdf	Emcdf	dEcal
<i>1s2s2p²3d⁶F_J-1s2p³3d⁶D_J</i>														
				± 106			± 167			± 385			± 783	
1/2-*	665.38	150290	665.83	150188	-102	666.07	150134	-156	663.74	150661	371	661.98	151062	772
3/2-*	665.65	150229	666.08	150132	-97	666.25	150094	-135	663.93	150618	389	662.18	151016	787
5/2-*	665.92	150168	666.32	150078	-90	666.56	150024	-144	664.25	150546	378	662.49	150946	777
7/2-*	666.27	150089	666.69	149995	-95	666.74	149984	-106	664.65	150455	366	662.88	150857	768
9/2-*	666.63	150008	667.10	149903	-106	667.35	149846	-162	665.08	150358	350	663.31	150759	751
11/2-9/2	666.99	149927	667.47	149819	-108	667.73	149761	-166	665.51	150261	333	663.72	150666	739
AVwei	666.41	150058	666.86	149957	-101	667.06	149911	-147	664.83	150415	357	663.06	150817	759
AVunw	666.14	150119	666.58	150019	-99	666.78	149974	-145	664.53	150483	364	662.76	150884	766
QED					-23.2			-23.2						
HO					270.8			84.6						
AVwei ^T			665.76	150205	147	666.79	149972	-86						
nonrel						670.72	149094	-964						
<i>1s2s2p²3d⁶D_J-1s2p³3d⁶D_J</i>														
				± 235			± 373			± 486			± 892	
1/2-*	686.42	145683	685.35	145911	227	688.18	145311	-373	684.20	146156	473	682.24	146576	893
3/2-*	686.39	145690	685.32	145917	227	688.15	145317	-373	684.18	146160	471	682.22	146580	891
5/2-*	686.39	145690	685.30	145921	232	688.15	145317	-373	684.47	146098	409	682.23	146578	888
7/2-*	686.51	145664	685.41	145898	234	688.27	145292	-372	684.27	146141	477	682.35	146552	888
9/2-*	686.87	145588	685.76	145824	236	688.63	145216	-372	684.71	146047	459	682.73	146471	883
AVwei	686.58	145649	685.49	145881	233	688.34	145276	-372	684.44	146105	456	682.43	146536	887
AVunw	686.52	145663	685.43	145894	231	688.28	145291	-372	684.37	146121	458	682.35	146551	888
QED					-23.1			-23.0						
HO					93.1			209.8						
AVwei ^T			685.16	145951	302	687.46	145463	-186						
nonrel						692.20	144467	-1182						
<i>1s2s2p²3d⁶P_J-1s2p³3d⁶D_J</i>														
				± 869			± 650			± 1705			± 590	
3/2-*	698.06	143254	693.88	144117	863	701.21	142611	-644	689.94	144940	1686	695.23	143837	583
5/2-*	698.57	143150	694.42	144005	855	701.76	142499	-651	690.42	144839	1690	695.76	143728	578
7/2-*	698.95	143072	694.73	143941	869	702.08	142434	-638	690.71	144779	1707	696.08	143662	590
AVwei	698.63	143138	694.25	144041	902	701.59	142534	-604	690.27	144871	1732	695.60	143762	624
AVunw	698.53	143158	694.34	144021	863	701.68	142514	-644	690.36	144853	1694	695.69	143742	584
QED					-23.0			-22.9						
HO					282.0			112.1						
AVwei ^T			693.00	144300	1162	701.15	142623	-515						
nonrel						705.59	141725	-1413						

In Table 5.3.1 all the observed lines in the sextet system of O IV are reported. Fourteen lines are new observations with the wavelength accuracy of $\pm 0.06 \text{ \AA}$. The quoted theoretical errors are the root mean square differences of the calculated and experimental values for the transition energies as given below in the table.

The strongest fine structure component is the $1s2s2p^23d \text{ } ^6F_{11/2} - 1s2p^33d \text{ } ^6D_{9/2}$ transition at the wavelength of $666.99 \pm 0.06 \text{ \AA}$. We also found the wavelengths for other $1s2s2p^23d \text{ } ^6L_J - 1s2p^33d \text{ } ^6D_J$, L=P, D, F transitions. Most of the new identifications have been obtained by searching in our spectra for sets of unidentified lines and by comparing the energies and relative intensities in agreement with our accurate MCHF and MCDF theoretical predictions. The transition rates are proportional to the area of the peaks (the fitted intensity \times FWHM of the experiments). We compared the measured transition rates with calculated results. They are consistent. In Table 5.3.1 we present our measured fine structure wavelength values and compare these with our different theoretical values for O IV. They are consistent.

Fig. 5.3.2 displays the identifications of the $1s2s2p^23d \text{ } ^6F_J - 1s2p^33d \text{ } ^6D_{J^*}$ transitions of O IV in the experimental spectrum of $^{20}\text{O}^+$ at the energy of 2.5 MeV. Here *'s represent all possible allowed J's of the upper states by the E1 transition selective rules. In Fig. 5.3.2 the line for the $1s2s2p^23d \text{ } ^6F_{7/2} - 1s2p^33d \text{ } ^6D_{J^*}$ transition of O IV and the $1s^22p3p \text{ } ^1D_2 - 1s^22p4d \text{ } ^1F_3$ transition are of O V at $666.27 \pm 0.06 \text{ \AA}$. The latter transition was identified at $666.819 \pm 0.03 \text{ \AA}$ [136]. In this work we could resolve the lines and improve the wavelength accuracy of the $1s^22p3p \text{ } ^1D_2 - 1s^22p4d \text{ } ^1F_3$ transition to $666.27 \pm 0.06 \text{ \AA}$. We also list our results in Table 5.3.2. For the $1s^22p3p \text{ } ^1D_2$ state there are different couplings,

$1s^2 2p(j=1/2) 3p(j'=3/2) {}^1D_2$ and $1s^2 2p(j=3/2) 3p(j'=1/2) {}^1D_2$. For the $1s^2 2p 4d {}^1F_3$ state there are different couplings, $1s^2 2p(j=1/2) 4d(j'=5/2) {}^1F_3$ and $1s^2 2p(j=3/2) 4d(j'=3/2) {}^1F_3$. Their energies are different. The MCHF method handles it in the different way and gives different values from the MCDF values. The MCHF calculation can only give the minimum energies among both configurations. In Table 5.3.2 the SCHF calculation gave a quite different wavelength. We studied the spectrum in the wavelength range around 600 Å and found a strong unidentified line located at 599.85 ± 0.06 Å. We assign it as the $1s^2 2p 3p {}^1D_2 - 1s^2 2p 4d {}^1F_3$ transition and also list it in Table 5.3.2.

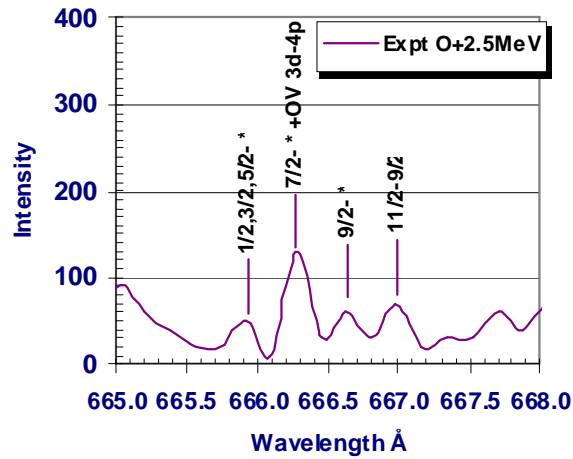


FIG. 5.3.2. The identifications of the $1s^2 2p^2 3d {}^6F_J - 1s^2 p^3 3d {}^6D_J$ transitions of O IV in the experimental spectrum of ${}^{20}\text{O}^+$ at the energy of 2.5 MeV.

TABLE 5.3.2. The wavelengths λ (in Å) for the $1s^2 2p 3p {}^1D_2 - 1s^2 2p 4d {}^1F_3$ transitions in O V by this work.

λ obs ^a	λ exp ^b	λ scdf ^a	λ mcdf ^a	λ schf ^a
± 0.06	± 0.03			
666.27	666.819	651.12	681.40	589.09
599.85		651.12	681.40	589.09

a this work

b [123]

5.3.2 The $1s2s2p^23d\ ^6L-1s2p^33d\ ^6D^o$ Transitions in F V.

We obtained spectra at a beam energy of 2.5 MeV for fluorine. In the wavelength region of 570-620 Å the transitions between the sextet states $1s2s2p^23d\ ^6L$ and $1s2p^33d\ ^6D$ in F V were expected. The spectrum in the wavelength region is shown in Fig. 5.3.1(d). A promising candidate for the $1s2s2p^23d\ ^6F_{11/2} - 1s2p^33d\ ^6D_{9/2}$ transition at 574.05 ± 0.10 Å appears at the 2.5 MeV (FH)⁺ ion beam energy. Nonlinear least square fits of Gaussian profiles gave the values for the wavelengths, intensities and full widths at half maximum (FWHM) of the lines. The uncertainties of the wavelengths are related to the intensities of the lines. Through the use of optical refocusing we achieved spectroscopic linewidth of 0.7 Å. The precision of the profile-fitting program was also checked through several known transition wavelengths. Using similar experimental analysis procedure as described above we obtained the wavelength accuracy of ±0.10 Å for the $1s2s2p^23d\ ^6L - 1s2p^33d\ ^6D$ transitions in the wavelength region of 570-620 Å.

In Table 5.3.3 all the observed lines in the sextet system of F V are reported. Fourteen lines are new observations. The strongest fine structure component is the $1s2s2p^23d\ ^6F_{11/2} - 1s2p^33d\ ^6D_{9/2}$ transition at the wavelength of 574.05 ± 0.10 Å. We also found other wavelengths for the $1s2s2p^23d\ ^6L_J - 1s2p^33d\ ^6D_J$, L=P, D, F transitions. We compared the measured transition rates with calculated results. They are consistent. In Table 5.3.3 we present our measured fine structure wavelength values and compare these with our different theoretical values for F V. They are consistent.

TABLE 5.3.3. The energies E (in cm^{-1}) and wavelengths λ (in \AA) for the $1s2s2p^23d\ ^6L_J-1s2p^33d\ ^6D_J$ transitions in FV by this work. We also list the deviations between the theoretical and experimental transition energies for the $1s2s2p^23d\ ^6L_J-1s2p^33d\ ^6D_J$ transitions.

J-J'	λ exp ± 0.10	Eexp	λ mchf	Emchf	dEcal	λ schf	E schf	dEcal	λ sclf	Esclf	dEcal	λ mclf	Emclf	dEcal
<i>1s2s2p²3d⁶F_J-1s2p³3d⁶D_J</i>														
				± 249			± 156			± 596			± 1041	
1/2-*	571.76	174899	571.40	175009	110	572.27	174743	-156	569.83	175491	592	568.94	175765	867
3/2-*	572.01	174822	571.64	174935	113	572.52	174666	-156	570.07	175417	595	568.17	176004	1182
5/2-*	572.41	174700	572.05	174810	110	572.92	174544	-156	570.48	175291	591	569.59	175565	865
7/2-*	572.91	174547	572.55	174657	110	573.42	174392	-155	571.02	175125	578	570.13	175399	851
9/2-*	573.48	174374	572.58	174648	274	573.99	174219	-155	571.62	174941	567	570.75	175208	834
11/2-9/2	574.05	174201	573.15	174474	274	574.56	174046	-155	572.23	174755	554	571.37	175018	817
AVwei	573.16	174471	572.52	174668	196	573.67	174316	-155	571.28	175044	573	570.31	175343	871
AVunw	572.77	174590	572.23	174755	165	573.28	174435	-155	570.88	175170	580	569.83	175492	902
QED				-41.1			-41.1							
HO				104.0			121.2							
AVwei ^T			572.31	174731	260	573.41	174396	-75						
nonrel						578.11	172977	-1494						
<i>1s2s2p²3d⁶D_J-1s2p³3d⁶D_J</i>														
				± 104			± 564			± 549			± 830	
1/2-*	591.85	168962	591.51	169059	97	593.83	168398	-563	589.97	169500	538	588.97	169788	826
3/2-*	591.82	168970	591.48	169067	97	593.80	168407	-563	589.93	169512	541	588.94	169797	826
5/2-*	591.86	168959	591.51	169059	100	593.84	168396	-563	589.96	169503	544	588.98	169785	826
7/2-*	592.05	168905	591.69	169007	103	594.03	168342	-563	590.14	169451	547	589.18	169727	823
9/2-*	592.52	168771	592.15	168876	105	594.50	168209	-562	590.70	169291	520	589.70	169578	807
AVwei	592.12	168883	591.77	168985	102	594.10	168321	-563	590.25	169419	536	589.27	169702	819
AVunw	592.02	168913	591.67	169014	100	594.00	168350	-563	590.14	169451	538	589.15	169735	822
QED				-40.8			-40.8							
HO				249.7			63.4							
AVwei ^T			591.04	169194	311	594.02	168344	-539						
nonrel						598.88	166978	-1905						
<i>1s2s2p²3d⁶P_J-1s2p³3d⁶D_J</i>														
				± 353			± 1861			± 1235			± 475	
3/2-*	604.10	165536	603.27	165763	228	610.97	163674	-1861	599.75	166736	1201	605.84	165060	-475
5/2-*	604.88	165322	603.99	165566	244	611.75	163465	-1857	600.45	166542	1220	606.60	164853	-469
7/2-*	605.36	165191	604.03	165555	364	612.22	163340	-1851	600.87	166425	1234	607.08	164723	-468
AVwei	604.64	165388	603.68	165651	263	611.51	163530	-1857	600.23	166602	1215	606.37	164916	-472
AVunw	604.78	165349	603.76	165628	278	611.65	163493	-1856	600.36	166568	1218	606.51	164879	-471
QED				-40.6			-40.5							
HO				53.0			175.8							
AVwei ^T			603.63	165663	275	611.00	163665	-1723						
nonrel						616.56	162190	-3197						

5.3.3 The $1s2s2p^23d\ ^6L-1s2p^33d\ ^6D^o$ Transitions in Ne VI.

We obtained spectra at a beam energy of 4.0 MeV for neon. In the wavelength region of 490-550 Å the transitions between the sextet states $1s2s2p^23d\ ^6L$ and $1s2p^33d\ ^6D$ in Ne VI were expected. The spectrum is shown in Fig. 5.3.1(e). For the $1s2s2p^23d\ ^6L-1s2p^33d\ ^6D$ transitions we expected to see the fine structures of the lower states $1s2s2p^23d\ ^6L$ in our experiments, whereas the fine structures of the upper states $1s2p^33d\ ^6D$ can also be partially resolved with the resolution of the experimental spectrum. A promising candidate for the $1s2s2p^23d\ ^6F_{11/2} - 1s2p^33d\ ^6D_{9/2}$ transition at 503.45 ± 0.05 Å appears in the spectrum recorded at the 4.0 MeV $^{20}\text{Ne}^+$ ion beam energy. Nonlinear least square fits of Gaussian profiles gave the values for the wavelengths, intensities and full widths at half maximum (FWHM) of lines. Through the use of optical refocusing we achieved spectroscopic linewidths of 0.4 Å in the second order spectrum. The precision of the profile-fitting program was checked through several known transition wavelengths. Using similar experimental procedures as described above, we obtained the wavelength accuracy of ± 0.05 Å for the $1s2s2p^23d\ ^6L - 1s2p^33d\ ^6D$ transitions in the wavelength region of 490-550 Å.

The strongest transition fine structure component is the $1s2s2p^23d\ ^6F_{11/2} - 1s2p^33d\ ^6D_{9/2}$ transition at the wavelength of 503.45 ± 0.05 Å. In Table 5.3.4 we present our measured fine structure wavelength values for the $1s2s2p^23d\ ^6L_J - 1s2p^33d\ ^6D_J$, L=P, D, F transitions for Ne VI and compare these with our different theoretical values. They are consistent. Fourteen lines are new observations.

TABLE 5.3.4. The energies E (in cm^{-1}) and wavelengths λ (in \AA) for the $1s2s2p^23d^6L_J-1s2p^33d^6D_J$ transitions in Ne VI by this work. We also list the deviations between the theoretical and experimental transition energies for the $1s2s2p^23d^6L_J-1s2p^33d^6D_J$ transitions.

J-J'	λ exp ± 0.05	Eexp	λ mchf	Emchf	dEcal	λ schf	E schf	dEcal	λ scdf	Escdf	dEcal	λ mcdf	Emcdf	dEcal
<i>1s2s2p²3d⁶F_J-1s2p³3d⁶D_J</i>														
				± 3448			± 180			± 811			± 946	
1/2-*	500.40	199840	492.42	203079	3239	500.79	199684	-156	498.37	200654	814	498.03	200791	951
3/2-*	500.66	199736	492.69	202967	3231	501.12	199553	-183	498.67	200533	797	498.35	200662	926
5/2-*	501.18	199529	493.12	202790	3261	501.62	199354	-175	499.18	200329	799	498.86	200457	928
7/2-*	501.84	199267	493.69	202556	3290	502.27	199096	-171	499.88	200048	781	499.54	200184	917
9/2-*	502.71	198922	494.26	202323	3401	503.03	198795	-127	500.69	199724	803	500.33	199868	946
11/2-9/2	503.45	198629	496.86	201264	2634	503.80	198491	-138	501.53	199390	760	501.17	199533	904
AVwei	502.23	199111	494.49	202227	3116	502.62	198959	-152	500.26	199897	786	499.91	200035	924
AVunw	501.71	199320	493.84	202495	3175	502.11	199162	-158	499.72	200112	792	499.38	200248	929
QED				-67.2			-67.1							
HO				94.1			-2.3							
AVwei ^T			494.43	202254	3143	502.79	198890	-221						
nonrel						508.95	196483	-2628						
<i>1s2s2p²3d⁶D_J-1s2p³3d⁶D_J</i>														
				± 2509			± 671			± 745			± 891	
1/2-*	519.65	192437	513.56	194719	2282	521.42	191784	-653	517.81	193121	684	517.41	193270	833
3/2-*	519.63	192445	513.55	194723	2278	521.41	191788	-657	517.78	193132	688	517.40	193274	829
5/2-*	519.70	192419	513.49	194746	2327	521.49	191758	-660	517.83	193114	695	517.48	193244	825
7/2-*	520.14	192256	513.57	194715	2459	521.75	191663	-593	518.10	193013	757	517.74	193147	891
9/2-*	520.81	192009	513.94	194575	2567	522.33	191450	-559	518.82	192745	736	518.39	192905	896
AVwei	520.17	192243	513.67	194676	2433	521.82	191635	-608	518.22	192967	724	517.84	193111	868
AVunw	519.99	192313	513.62	194696	2383	521.68	191688	-624	518.07	193025	712	517.68	193168	855
QED				-66.7			-66.6							
HO				-16.5			-85.3							
AVwei ^T			513.89	194593	2350	522.24	191483	-760						
nonrel						527.59	189541	-2702						
<i>1s2s2p²3d⁶P_J-1s2p³3d⁶D_J</i>														
				± 8011			± 1274			± 2526			± 273	
3/2-*	537.00	186220	517.23	193338	7118	540.69	184949	-1271	530.01	188676	2456	536.33	186452	233
5/2-*	538.10	185839	518.34	192924	7085	541.74	184590	-1249	530.92	188352	2513	537.32	186109	270
7/2-*	538.69	185636	529.08	189007	3372	542.39	184369	-1266	531.50	188147	2511	537.94	185894	259
AVwei	537.74	185963	520.23	192221	6259	541.42	184700	-1262	530.64	188450	2487	537.02	186214	251
AVunw	537.93	185898	521.55	191736	5838	541.61	184636	-1262	530.81	188391	2494	537.20	186152	254
QED				-66.4			-66.2							
HO				-100.4			-219.8							
AVwei ^T			520.69	192054	6091	542.26	184414	-1549						
nonrel						547.62	182608	-3354						

5.3.4 Comparisons with Theory of the $1s2s2p^23d\ ^6L - 1s2p^33d\ ^6D$ Transitions along *B I Isoelectronic Sequence*

In order to verify the validity of our experimental and theoretical approaches above, we have studied the deviations between the experimental and theoretical transition energies of the $1s2s2p^23d\ ^6L - 1s2p^33d\ ^6D$ transitions along the boron isoelectronic sequence. In Figs. 5.3.3, 5.3.4 and 5.3.5 we show plots of the deviations between the theoretical and experimental transition energies of the $1s2s2p^23d\ ^6L - 1s2p^33d\ ^6D$, L=P, D, F transitions for boron-like ions. Here, the theoretical transition energy is the center of gravity of the $1s2s2p^23d\ ^6L_J - 1s2p^33d\ ^6D_J$ transition energies (computed from the fine structure lines by this work) with the results of theoretical analysis, and the experimental transition energy is the center of gravity of the $1s2s2p^23d\ ^6L_J - 1s2p^33d\ ^6D_J$ transition energies (computed from the observed lines) with the results of experimental analysis. In Fig. 5.3.3 the MCDF, SCHF and SCDF deviations are constant for all $1s2s2p^23d\ ^6F - 1s2p^33d\ ^6D$ transitions with nuclear charge $Z = 8, 9$ and 10 . The non-relativistic SCHF deviations are linear. The MCHF deviations of oxygen and fluorine are small, just 106 and 249 cm^{-1} .

In Fig. 5.3.4 the SCHF, SCDF and MCDF deviations are constant for all $1s2s2p^23d\ ^6D - 1s2p^33d\ ^6D$ transitions with nuclear charge $Z = 8, 9$ and 10 . The non-relativistic SCHF deviations are linear. The MCHF deviations of oxygen fluorine are small, just 235 and 104 cm^{-1} .

In Fig. 5.3.5 the SCHF and MCDF deviations are constant for all $1s2s2p^23d\ ^6P - 1s2p^33d\ ^6D$ transitions with nuclear charge $Z = 8, 9$ and 10 . The SCDF and non-relativistic SCHF deviations are linear. These smoothly varying linear or

constant energy deviations can be used to predict easily and with high accuracy the transition energies for the $1s2s2p^23d\ ^6L - 1s2p^33d\ ^6D$, $L=P, D, F$ transitions for boron-like ions with $5 < Z < 13$.

In Figs. 5.3.6, 5.3.7 and 5.3.8 we summarize the detailed results of the fine structures of the $1s2s2p^23d\ ^6L_J$, $L=F, D, P$ states for O IV, F V and Ne VI. The comparisons of the measured fine structures of the $1s2s2p^23d\ ^6L_J$ states show reasonable agreement. Here, the error bars are from experiments.

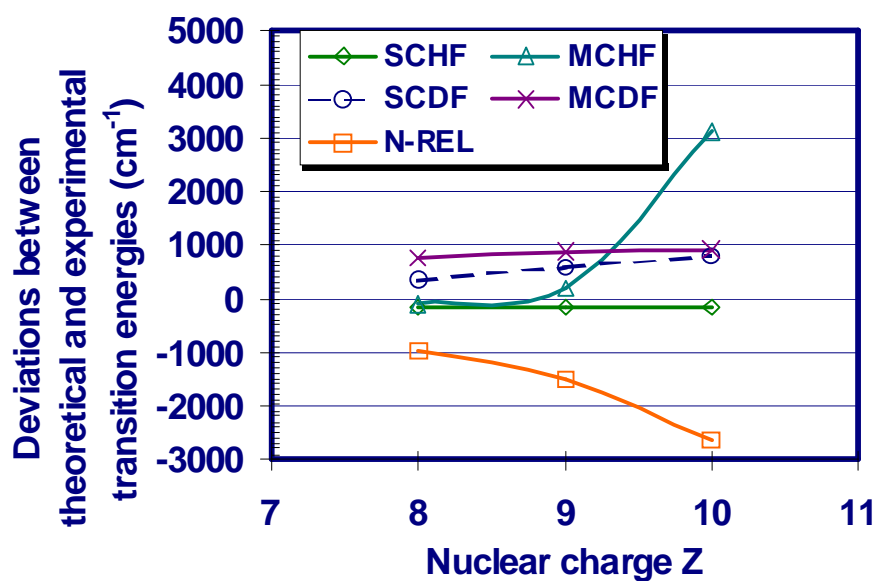


FIG. 5.3.3. The deviations between the theoretical and experimental transition energies for the $1s2s2p^23d\ ^6F - 1s2p^33d\ ^6D$ transitions.

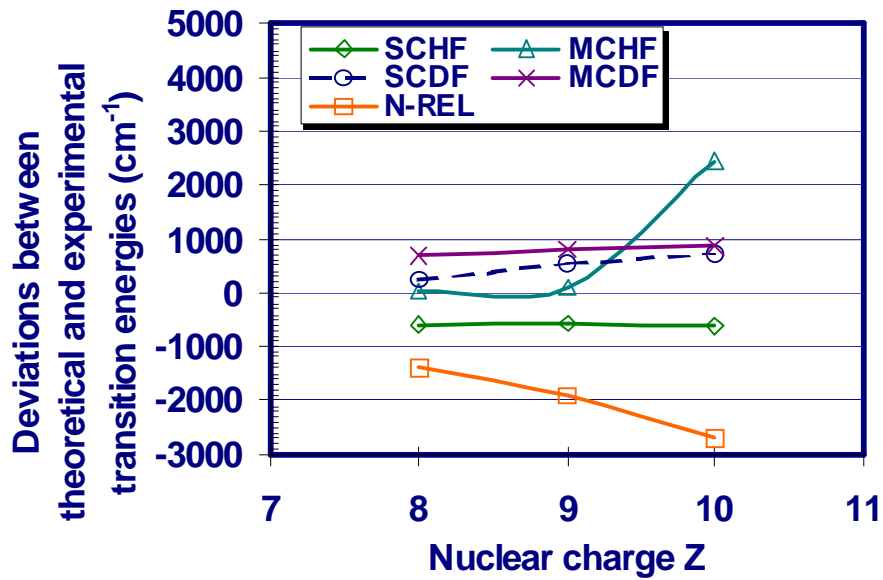


FIG. 5.3.4. The deviations between the theoretical and experimental transition energies for the $1s2s2p^2 3d^6 D-1s2p^3 3d^6 D$ transitions.

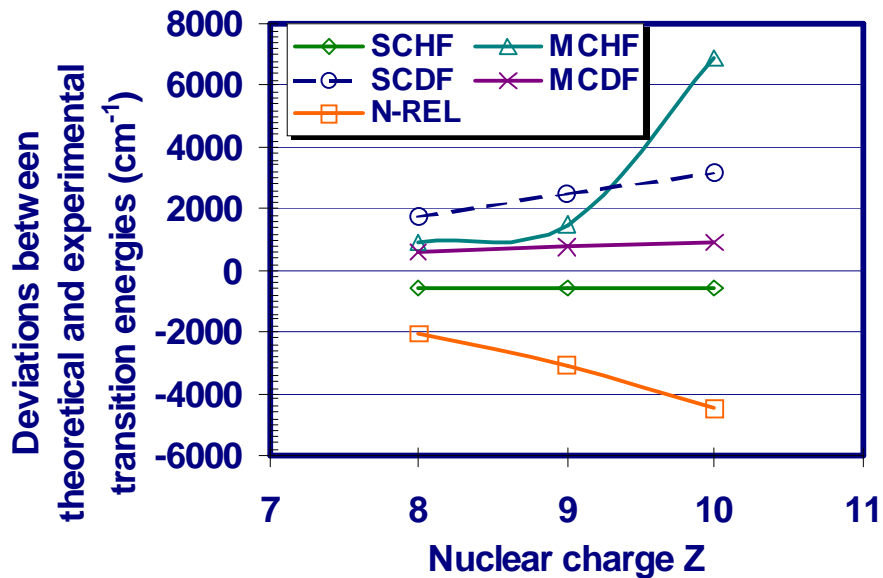


FIG. 5.3.5. The deviations between the theoretical and experimental transition energies for the $1s2s2p^2 3d^6 P-1s2p^3 3d^6 D$ transitions.

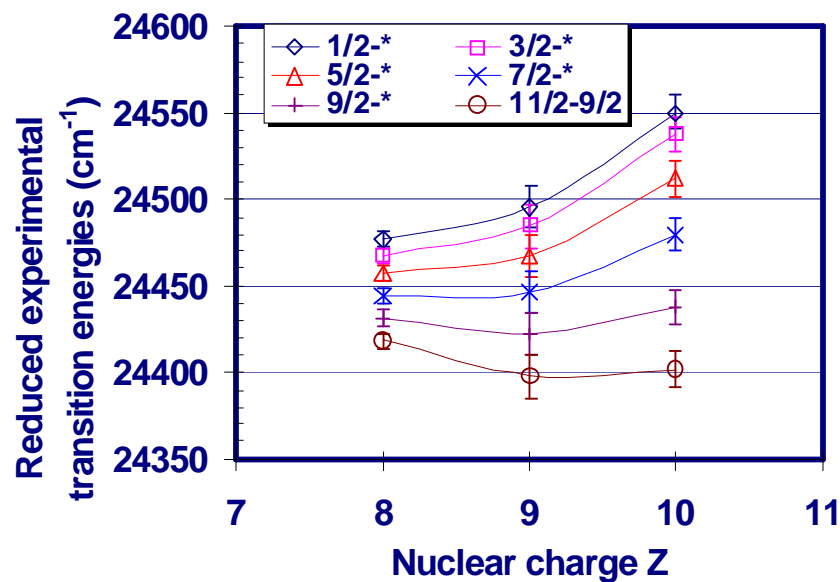


FIG. 5.3.6. The reduced experimental transition energies $\Delta E/(Z-1.86)$ for the $1s2s2p^2 3d {}^6F_J-1s2p^3 3d {}^6D_J$ transitions.

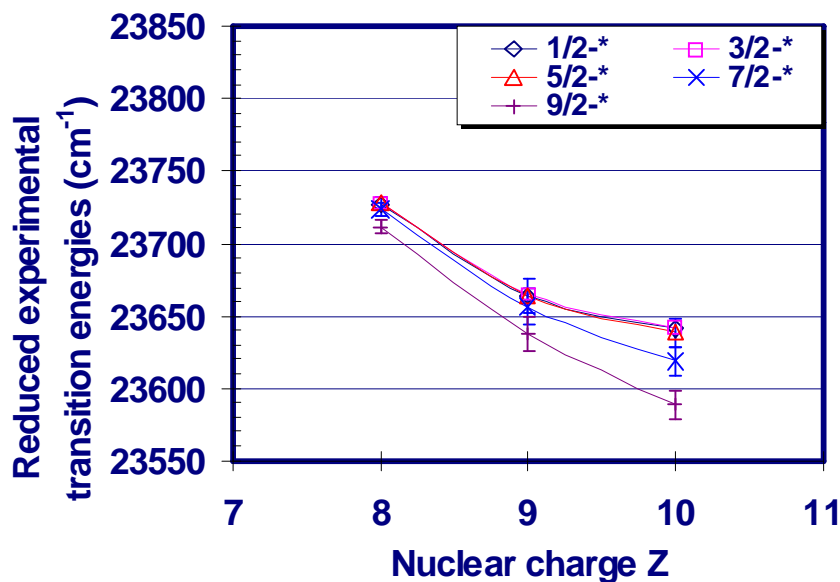


FIG. 5.3.7. The reduced experimental transition energies $\Delta E/(Z-1.86)$ for the $1s2s2p^2 3d {}^6D_J-1s2p^3 3d {}^6D_J$ transitions.

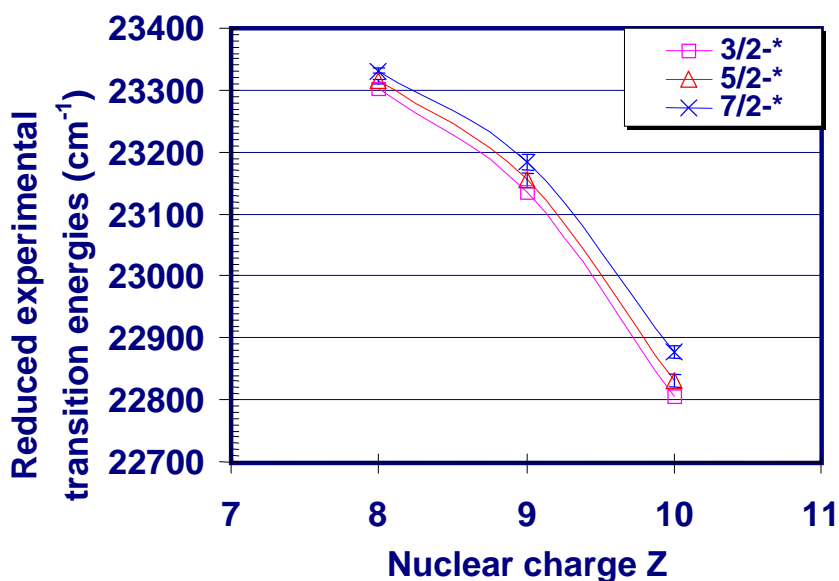


FIG. 5.3.8. The reduced experimental transition energies $\Delta E/(Z-1.86)$ for the $1s2s2p^23d$ ${}^6P_J-1s2p^33d$ 6D_J transitions.

Our MCHF, SCHF and MCDF calculated lifetime results for the $1s2s2p^23d$ 6P and $1s2p^33d$ 6D states for N III, O IV and F V are in good agreement with the measurements by Blanke et al [51] and the calculations of Miecznic [16] et al (see Table 5.3.5 and Figs. 5.3.9 and 5.3.10). The discrepancies between theory and experiments are close to the value of experimental precisions. The discrepancies are most probably due to the additional decay modes of M2 and radiative autoionization or some missing configurations which are important for MCHF and MCDF calculations. In Table 5.3.5 we also list our calculated lifetime results for the $1s2s2p^23d$ 6P states for Ne VI and Na VII and for the $1s2p^33d$ 6D states for N III, O IV, F V, Ne VI and Na VII.

TABLE 5.3.5. Lifetimes (in ps) of the $1s2s2p^23d\ ^6P$ and $1s2p^33d\ ^6D$ states in N III, O IV, F V, Ne VI and Na VII.

Ion	This work			Experiment	Theory
	MCHF	SCHF	MCDF		
<i>$1s2s2p^23d\ ^6P$</i>					
N III	45.37	40.65	47.42	51 ± 12^a	42.8 ± 18^b
O IV	15.32	15.29	16.01	12 ± 3^a	14.95 ± 4^b
F V	6.82	6.90	7.02	11 ± 4^a	6.689 ± 4^b
Ne VI	3.57	3.54	3.61		
Na VII	2.1	2.04	2.07		
<i>$1s2p^33d\ ^6D$</i>					
N III	275.3	286.2	255.3		
O IV	225.7	238.7	213.1		
F V	196.7	204.3	183.3		
Ne VI	170.1	178.1	153.0		
Na VII	150.8	157.4	140.0		

a Blanke [15].

b Miecznik [16].

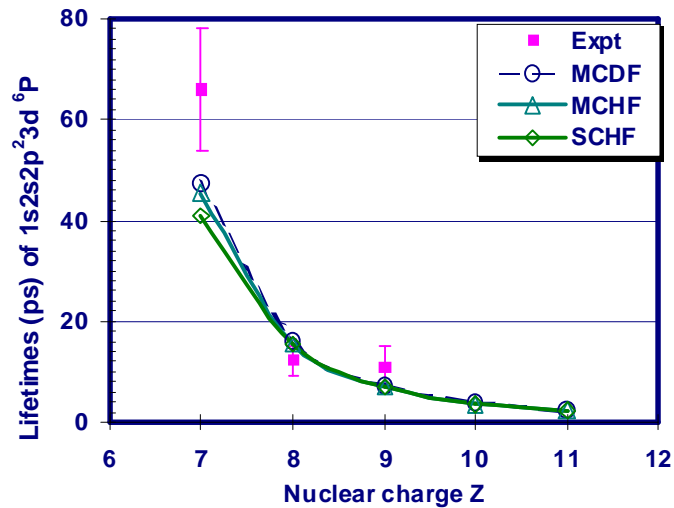


FIG. 5.3.9. The lifetimes (in ps) for the $1s2s2p^23d\ ^6P^e$ states in the boron sequence. Experimental values are taken from Table 5.3.5.

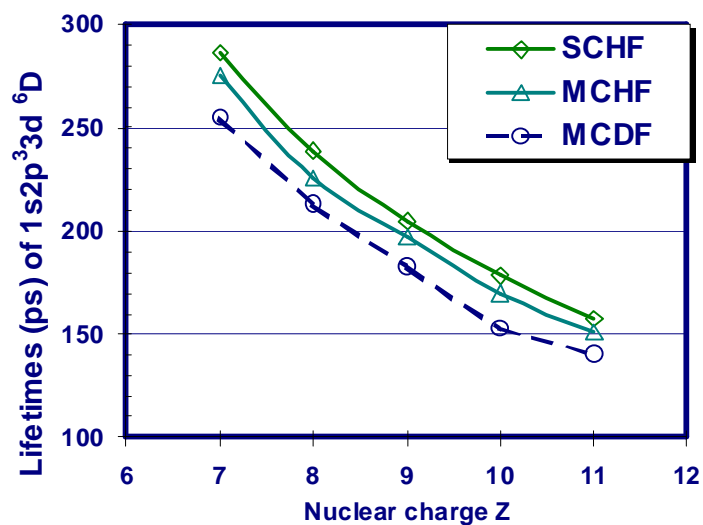


FIG. 5.3.10. The lifetimes (in ps) for the $1s2p^3 3d \ ^6D^o$ states in the boron sequence.

The QED and higher-order corrections for the $1s2s2p^2 3d \ ^6L$, $L=F, D, P$ - $1s2p^3 3d \ ^6P$ transitions in O IV, F V and Ne VI are up to -220 - 370 cm^{-1} (see Table 5.3.1, 5.3.3 and 5.3.4) and can't be ignored in the careful comparisons with experiments. Here, the QED and higher-order corrections were calculated from the effective nuclear charge Z_{eff} obtained from the MCHF and SCHF calculations. In Fig. 5.3.11 we plot the above corrections to the weighted mean transition energies. The results show that the weighted mean wavelengths for the $1s2s2p^2 3d \ ^6L$, $L=F, D, P$ - $1s2p^3 3d \ ^6P$ transitions in O IV, F V and Ne VI are sensitive to the QED and higher-order corrections to 0.27 \AA , 0.26 \AA and 0.18 \AA , respectively. They are larger than our estimated experimental precision of $\pm 0.06 \text{ \AA}$, $\pm 0.10 \text{ \AA}$ and $\pm 0.05 \text{ \AA}$. Here, the transition energies are strongly related to the electron correlation. We could not obtain the exact electron correlation. The QED and higher-order corrections in the sextet states of boron-like systems are large enough to be seen experimentally. This work provides a good test for the

QED and higher-order corrections if the theory of the electron correlation is well known.

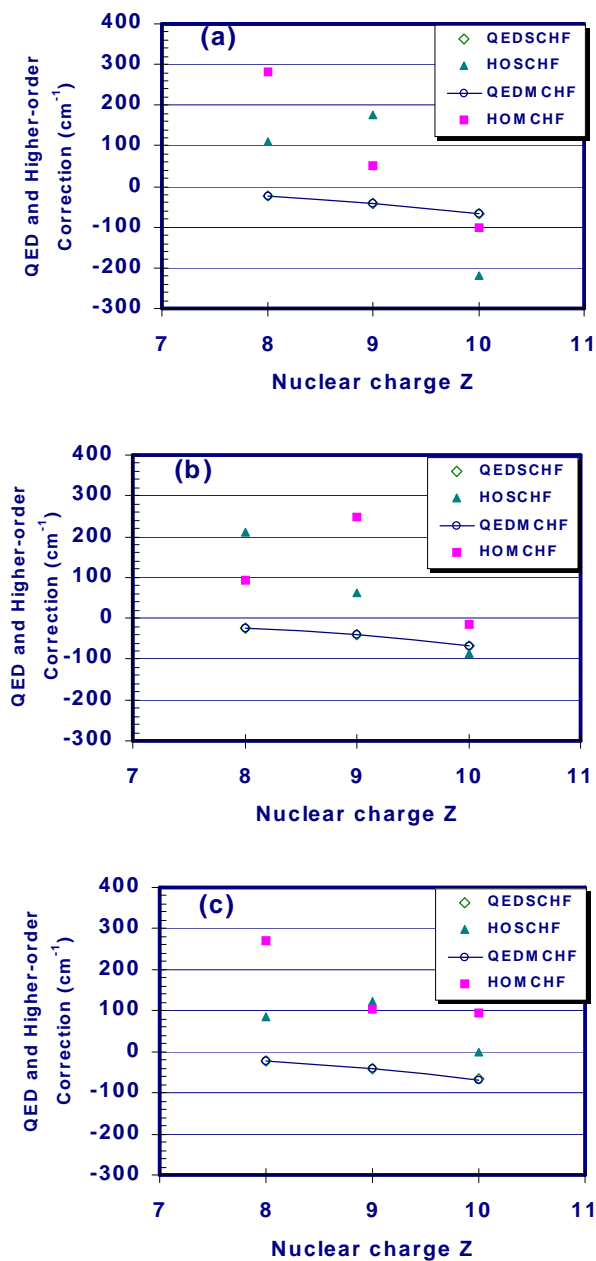


FIG. 5.3.11. The QED and higher-order corrections for (a) the $1s2s2p^23d\ ^6F-1s2p^33d\ ^6D$, (b) $1s2s2p^23d\ ^6D-1s2p^33d\ ^6D$ and (c) $1s2s2p^23d\ ^6P-1s2p^33d\ ^6D$ transitions in the B I isoelectronic sequence.

5.3.5. Summary

We performed MCHF (with QED and higher-order corrections) and MCDF calculations for the $1s2s2p^23d \ ^6L-1s2p^33d \ ^6D$, $L=P, D, F$ electric-dipole transitions of five-electron O IV, F V and Ne VI. The present beam-foil study of oxygen, fluorine and neon led to the observations of 42 new lines in the sextet system of O IV, F V and Ne VI. We measured the wavelengths with good accuracy. They are in excellent agreement with our recent theoretical results by this work. Identifications are verified mainly due to the fact that the theoretical transition energy deviations from the experiments are in the reasonable range.

Moreover, it has been possible to classify many newly observed lines in O IV, F V and Ne VI by calculating the wavelengths of transitions between the known sextet energy levels from above sections.